

# **Measuring Rapid Kinetics by Electroanalytical Methods in Droplet-based Microfluidic Devices**

HAN, Zuoyan

A Thesis Submitted in Partial Fulfillment  
of the Requirements for Degree of  
Doctor of Philosophy  
in  
Chemistry

The Chinese University of Hong Kong  
August 2011

UMI Number: 3500840

All rights reserved

INFORMATION TO ALL USERS

The quality of this reproduction is dependent on the quality of the copy submitted.

In the unlikely event that the author did not send a complete manuscript and there are missing pages, these will be noted. Also, if material had to be removed, a note will indicate the deletion.



UMI 3500840

Copyright 2012 by ProQuest LLC.

All rights reserved. This edition of the work is protected against unauthorized copying under Title 17, United States Code.



ProQuest LLC.  
789 East Eisenhower Parkway  
P.O. Box 1346  
Ann Arbor, MI 48106 - 1346

## Thesis/Assessment Committee

Professor Man Chor Chan (Chair)

Professor Bo Zheng (Thesis Supervisor)

Professor Shannon Wing Ngor Au (Committee Member)

Professor Xingyu Jiang (External Examiner)

Professor Zongwei Cai (External Examiner)

Abstract of the thesis entitled:

## **Measuring Rapid Kinetics by Electroanalytical Methods in Droplet-Based Microfluidic Devices**

Submitted by HAN, Zuoyan

for the degree of Doctor of Philosophy

at The Chinese University of Hong Kong in August 2011

### **Abstract (English)**

This thesis describes a droplet-based microfluidic system with pneumatic valves for measuring rapid kinetics using electroanalytical methods. Aqueous streams containing the reactants are injected into a flow of immiscible oil in microchannels to generate nanoliter droplets and to initiate the reaction inside the droplets. By flowing the droplets through a winding channel, chaotic mixing within milliseconds can be achieved due to the secondary flow inside the droplets. Pneumatic valves were used to control the travelling distance and in turn the reaction time of the droplets. Microelectrodes were integrated at the outlet of the microchannel for measuring the rapid kinetics. Two important electroanalytical techniques, potentiostatic and potentiometric, were applied in the droplet-based microfluidic systems to monitor the enzymatic kinetics of catalase and binding kinetics of RNA-Mg<sup>2+</sup> system respectively.

The thesis contains two major parts. In the first part, millisecond enzyme kinetics was studied using amperometric detection method. A complete Michaelis-

Menten kinetics of catalase was successfully measured by amperometric method in a single-run experiment, and the total consumption of reagents was less than 50  $\mu\text{L}$ . In the current experiment, the best time resolution was about 0.05 s, and the reaction time measured was from 0.05 s to 25 s. This microfluidic system with amperometric method is applicable to many biochemical reactions, as long as one of the reactants or products is electrochemically active.

The second part reports the development of the potentiometric detection method in droplet-based microfluidic system by integration of a group of phase separation channels. The phase separation channels separate oil phase between the aqueous droplets and form a continuous aqueous phase, which facilitates the potentiometric measurement by ion selective electrodes. RNA-Mg<sup>2+</sup> binding kinetics was monitored by measuring Mg<sup>2+</sup> ion concentration. The total consumption of RNA sample was less than 20  $\mu\text{L}$  and the best time resolution achieved currently was less than 0.1 s. The integration of ion selective electrodes with the droplet-based microfluidics extends the application of electroanalytical methods in biochemical and biophysical research, where measurements of a specific ionic concentration in small volumes of samples are required.

## Abstract (Chinese)

這篇論文主要研究了如何將電化學分析方法應用於在微流體芯片中以實現檢測快速反應動力學。首先微管道中含有反應物的溶液與不互溶的油相形成納升級的微液滴，在通過一段彎曲的微管道後，由於混沌的作用實現了微秒級的快速混合。通過利用在微管道中加入氣動閥門單元來控制微液滴在微管道中的行駛距離，從而控制微液滴中反應物的反應時間。同時利用在微管道出口處加入的微電極來實現檢測快速動力學。這篇論文主要用了電流測定 (Amperometry) 和電勢測定 (Potentiometry) 兩種方法，分別實現了過氧化氫酶反應動力學以及 RNA-Mg<sup>2+</sup> 結合動力學的檢測。

論文第一部分利用電流測定法實現了微秒級酶反應動力學的測定。在一次實驗中，只需要少於 50 微升的反應物就可以得到過氧化氫酶的 Michaelis-Menten 動力學。基於目前的實驗方法，可以檢測 0.05 秒至 25 秒的動力學，時間分辨率為 0.05 秒。利用電流測定法，微流體芯片實現了許多有電化學活性的生物化學反應的檢測。

第二部分通過在微流體芯片中引入一組相分離微管道以實現電勢測定法。疏水的相分離微管道可以將連續的油相分離，油相中單分散的微液滴形成連續的水相，有利於離子選擇性電極的檢測。通過檢測 Mg<sup>2+</sup> 的濃度，實現了 RNA-Mg<sup>2+</sup> 結合動力學的測定。整個實驗中使用的 RNA 樣品少於 50 微克，時間分辨率小於

0.1 秒。通過離子選擇性電極的加入，微流體芯片實現了生物化學體系微量樣品中離子的檢測。

這篇論文主要通過將不同的電化學分析方法應用到微流體技術中，結合電化學和微流體的優勢來解決生物化學體系中微量樣品的快速反應動力學研究。電化學微流體芯片將在研究許多沒有熒光或者顏色變化的反應體系中有廣泛的應用前景。

## Acknowledgements

I would like to take this opportunity to thank many people for helping me during my PhD research. I could never have finished the same without their kind support and encouragements.

In the first place I would like to give my profound gratitude to my mentor Prof. Bo Zheng for his supervision, advice, and guidance. Above all and the most needed, he provided me encouragement and support in various ways. His truly scientist intuition exceptionally inspire and enrich my growth as a student. I am indebted to him more than he knows.

I would like to thank Dr. Feng Shi for her helpful discussion and techniques in syringe pumps and fluorescence microscope. I am much appreciated for Dr. Xuechang Zhou's valuable advice in science discussion and guidance in photolithography. I would like to thank Huan Liu for her kindly discussion of ion-selective electrodes, which is of great help for this research work. I gratefully thank Dameng Guo, who helped me with the design the experiment of RNA-Mg<sup>2+</sup> binding kinetics. Special thanks also give to two undergraduates, Yuen Yan Chang and Mengwen Zhang for their outstanding works in RNA synthesis and analysis. I have also benefited from constructive advices from Xiaoju Tang, Xiaohu Zhou Yuefang Li, Yimeng Zhao and Hui Feng.

I would also acknowledge Prof. Yanyi Huang and his students Wentao Li at Peking University for their willingness to share the knowledge of multilayer microfluidics and pneumatic valves, which are very important to my research. I am very appreciated Prof. Shannon Au from Department of Biochemistry, who herself taught me

the basics of biotechnologies. I learnt a lot from her. I would like to thank Prof. Yuanhua Shao from Peking University for his broad knowledge and helpful discussion about electrochemistry. I also thank Prof. Lei Xu from Department of Physics, who generously provided us his state-of-the-art fast camera for recording the droplets movement at milliseconds scale.

My parents deserve special mention for their support. My Father, Xuezhi Han, in the first place is the person who put the fundament my learning character, showing me the joy of intellectual pursuit ever since I was a child. My Mother, Zheming Shou, is the one who sincerely raised me with her caring and gently love. Words fail me to express my appreciation to my wife Yan Ma for her dedication, love and persistent confidence in me, and furthermore for her precious times to read this thesis and gave her critical comments about it.

Finally, I would like to thank everybody who was important to the successful realization of thesis, as well as expressing my apology that I could not mention personally one by one.

Zuoyan Han

Hong Kong, June, 2011

## Table of Contents

<b>Abstract (English)</b> .....	<b>i</b>
<b>Abstract (Chinese)</b> .....	<b>iii</b>
<b>Acknowledgements</b> .....	<b>v</b>
<b>Table of Contents</b> .....	<b>vii</b>
<b>List of Figures</b> .....	<b>x</b>
<b>Chapter 1 Introduction</b> .....	<b>1</b>
<b>1.1 Chemical kinetics</b> .....	<b>1</b>
<b>1.2 PDMS-based microfluidics</b> .....	<b>4</b>
1.2.1 Multilayer microfluidics and pneumatic valves.....	6
1.2.2 Droplet-based microfluidic systems.....	7
1.2.3 Kinetics studies based on microfluidic systems .....	9
<b>1.3 Electroanalytical detection methods</b> .....	<b>12</b>
1.3.1 Potentiostatic techniques .....	12
1.3.2 Potentiometric techniques .....	13
1.3.3 Application of microelectrodes in integrated microfluidics .....	13
<b>Chapter 2 Measuring rapid enzymatic kinetics by amperometric method in droplet-based microfluidic device</b> .....	<b>16</b>
<b>2.1 Introduction of enzymatic kinetics and Michaelis-Menten Equation</b> .....	<b>16</b>
2.1.1 Enzyme kinetics.....	16
2.1.2 Michaelis-Menten kinetics .....	17

<b>2.2 Experimental.....</b>	<b>20</b>
2.2.1 Fabrication of microelectrodes .....	20
2.2.2 Fabrication of multilayer microfluidics with pneumatic valves .....	20
2.2.3 Sample preparation and operation .....	22
<b>2.3 Results and discussion .....</b>	<b>24</b>
2.3.1 Control of reaction time in droplets.....	24
2.3.2 Rapid mixing .....	25
2.3.3 Electrochemistry of hydrogen peroxide in microchannels.....	28
2.3.4 Analysis of the enzymatic kinetics.....	34
<b>2.4 Conclusions.....</b>	<b>40</b>
<b>Chapter 3 Measuring RNA-Mg<sup>2+</sup> binding kinetics by potentiometric method in droplet-based microfluidic device.....</b>	<b>41</b>
<b>3.1 Introduction of Mg<sup>2+</sup> induced RNA folding and its kinetics.....</b>	<b>41</b>
3.1.1 The concept of ion binding .....	41
3.1.2 <i>Tetrahymena</i> group I ribozyme.....	43
<b>3.2 Experimental.....</b>	<b>45</b>
3.2.1 Fabrication of micro Mg <sup>2+</sup> -selective electrode .....	45
3.2.2. Fabrication of the Microfluidic Devices .....	46
3.2.3 Preparation of P4-P6 domain of the <i>Tetrahymena</i> group I ribozyme .....	48
3.2.4 Instrumentation for the potentiometric measurements.....	48
<b>3.3 Results and discussion .....</b>	<b>49</b>
3.3.1 Integration of Mg <sup>2+</sup> selective microelectrode in microfluidic devices .....	49
3.3.2 Analysis of RNA-Mg <sup>2+</sup> binding kinetics .....	51
<b>3.4 Conclusions.....</b>	<b>56</b>

<b>Chapter 4 Conclusions and Perspectives.....</b>	<b>57</b>
<b>Appendix A Multilayer microfluidics fabrication.....</b>	<b>59</b>
<b>Appendix B. RNA synthesis.....</b>	<b>65</b>
<b>References.....</b>	<b>76</b>

## List of Figures

<i>Figure 1.1 A schematic of stopped-flow method.</i> .....	3
<i>Figure 1.2 A brief mechanism for peroxide-based PDMS cross-linking.</i> .....	5
<i>Figure 1.3 A brief mechanism for platinum-based PDMS cross-linking.</i> .....	5
<i>Figure 1.4 A schematic of pneumatic valves fabricated with PDMS membranes.</i> .....	7
<i>Figure 1.5 Schematic comparison of a reaction A + B conducted in a standard pressure-driven microfluidic system device (a) and in droplet-based microfluidic device (b).<sup>22</sup></i> .....	8
<i>Figure 1.6 (a) A schematic of the diffusive mixer.<sup>8</sup> (b) Left: a schematic of the microfluidic network. Right: a false-color fluorescence microphotograph.<sup>9</sup></i> .....	10
<i>Figure 2.1 Effect of substrate concentration on the initial velocity of an enzyme-catalyzed reaction.</i> ....	18
<i>Figure 2.2 A scheme of the fabrication of multilayer microfluidic devices.</i> .....	20
<i>Figure 2.3 Multilayer microfluidics for enzymatic kinetics experiments.</i> .....	22
<i>Figure 2.4 Microphotograph of the droplets moving along different routes controlled by pneumatic valves.</i> .....	25
<i>Figure 2.5 Rapid mixing was achieved with winding channels.</i> .....	27
<i>Figure 2.6 Current profile measured at 0.6 V (vs. Ag/AgCl quasi-reference electrode) for H<sub>2</sub>O<sub>2</sub> concentration ranging from 10 mM to 200 mM.</i> .....	29
<i>Figure 2.7 A serial of microphotographs showing droplets passing through the two microelectrodes.</i> ...30	30
<i>Figure 2.8 A series of microphotographs showing droplets passing by the two stainless steel wires (diameter ~ 20 μm), which were extended laterally across the microchannel.</i> .....	31
<i>Figure 2.9 A series of microphotographs showing droplets passing by the two stainless steel wires (diameter ~ 20 μm), which were extended laterally to only the middle of the microchannel.</i> .....	32
<i>Figure 2.10 Calibration of microelectrodes with different flow rates and H<sub>2</sub>O<sub>2</sub> concentrations.</i> .....	34
<i>Figure 2.11 The Selwyn plot for catalase.</i> .....	36
<i>Figure 2.12 Calibration curves of the current versus H<sub>2</sub>O<sub>2</sub> concentration before (blue squares) and after Selwyn's test (red triangles).</i> .....	36

Figure 2.13 Plots for Michaelis-Menten kinetics analysis.....	38
Figure 2.14 Plot of initial velocity ( $V$ ) vs. different substrate concentrations ( $[H_2O_2]$ ) at the same catalase concentration ( $10 \mu\text{g/mL}$ ).....	39
Figure 3.1 Modes of ion binding to RNA.....	42
Figure 3.2 Tetrahymena group I ribozyme secondary structures.....	44
Figure 3.3 A scheme of the fabrication of solid-contact ion-selective microelectrode.....	46
Figure 3.4 Multilayer microfluidics for RNA- $Mg^{2+}$ binding kinetics experiments.....	47
Figure 3.5 Potential measurement by $Mg^{2+}$ -selective microelectrode.....	50
Figure 3.6 Microphotographs of droplets passing through the two microelectrodes.....	51
Figure 3.7 RNA- $Mg^{2+}$ binding kinetics results.....	53
Figure 3.8 Calibration curve for $Mg^{2+}$ concentration measurement ranging from 0.03 mM to 3 mM with the linear fitting of the experimental data.....	54
Figure 3.9 Fitting results of the same data set from Figure 3.7b, d with single exponential, $Y = 1 - e^{-kt}$ .....	55

## Introduction

### Chapter 1 Introduction

#### 1.1 Chemical kinetics

Chemical kinetics deals with the rates of chemical reactions, factors that influence the rates and the explanation of the rates in terms of the reaction mechanisms of chemical processes. Chemical kinetics is different from chemical equilibria, which are governed by thermodynamics without concerning the intermediate states or time. In chemical kinetics, the time variable is introduced and rate of change of concentration of reactants or products with respect to time is followed. The chemical kinetics is thus concerned with the quantitative determination of rate of chemical reactions and of the factors upon which the rates depend. With the knowledge of effect of various factors, such as concentration, pressure, temperature, medium, effect of catalyst etc., on reaction rate, one can consider an interpretation of the empirical laws in terms of reaction mechanism.

The rate or velocity of a reaction ( $v$ ) may be expressed in terms of any one of the reactants or the products of the reaction. For example, in a bimolecular elementary reaction  $A+B \rightarrow C$ , in terms of molar concentrations

$$v = -\frac{d[A]}{dt} = -\frac{d[B]}{dt} = \frac{d[C]}{dt} = k[A][B]$$

where constant  $k$ , relating rate with concentration terms, is known as rate constant or velocity constant at a given temperature.

## Introduction

A kinetic study requires the determination of the concentration of the reactant or product as a function of time. The reaction rate ranges from femtosecond to minutes or even longer. Different reaction rate requires different techniques of kinetic study. For example, with ultrafast laser spectroscopy, it is now possible to study the reactions occurring in a few picoseconds ( $\sim 10^{-12}$  s).<sup>1</sup> The techniques, which have been designed to monitor concentrations and to measure the rate coefficients, include flash photolysis, relaxation methods and flow techniques. The other techniques including shock tubes and molecular beams have been used to explore the dependence of reaction rate on the state of rotational / vibrational excitation of molecules or on the energy with which molecules collide and the rate at which the energy is changed from one form into another. In the meanwhile, there are some conventional physical methods used to study the kinetics of slower reactions, which usually take seconds or minutes to complete, such as conductometric method, potentiometric method, spectrophotometry, fluorescence method, optical method and so on.

Recently, the developments in chemical kinetics have been a great interest in the study of rapid reactions that complete in less than 1 s. Rapid kinetics measurement is essential for understanding many biological and chemical processes, such as protein and RNA folding, protein-protein interaction, and enzymatic mechanism. For rapid kinetics within microseconds to seconds, stopped-flow<sup>2,3</sup> (Figure 1.1) and quenched-flow<sup>4,5</sup> are the two most often used measurement methods. In both methods, two or more reactant solutions are rapidly mixed in a mixing chamber. At desired reaction time, the flow is either stopped or quenched, and the reaction can be monitored using an appropriate

## Introduction

detection method. Both of these techniques provide fast mixing and short dead time for studying rapid kinetics. However, the conventional instrumentation using these two methods consumes large volumes of samples, which are not compatible with bioanalysis as the reagents are usually expensive or in limited supply. To solve the problem, many microfluidics systems were developed to study rapid kinetics in microchannels or microreactors.<sup>6-9</sup>

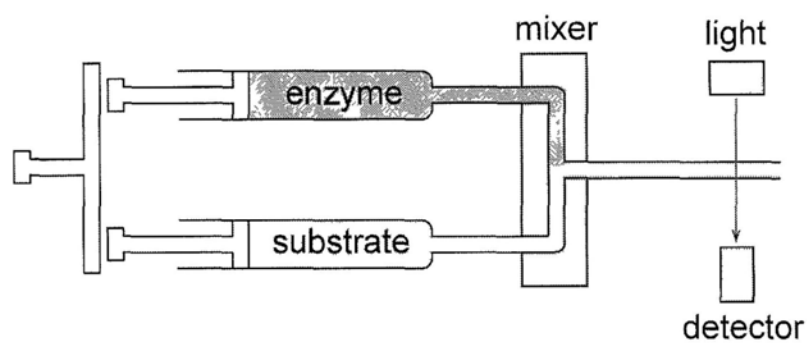


**Figure 1.1** A schematic of stopped-flow method.

## Introduction

### 1.2 PDMS-based microfluidics

Microfluidics are platforms developed for biological analysis, clinical diagnostics and drug screening. Microfluidics usually contain elements for the transportation, mixing, separation, and detection of samples. These elements are miniaturized to manipulate fluids in microchannels of tens to hundreds of microns. Microfluidic devices are usually fabricated in glass, silicon, and various plastics. Among these materials, polydimethylsiloxane (PDMS) is the most often used due to the low cost, simple fabrication procedure and the excellent optical transparency.<sup>10</sup>

PDMS is a silicone-based elastomer. PDMS is usually synthesized by cross-linking reactions initiated by organic peroxides (Figure 1.2) or platinum catalysts (Figure 1.3). PDMS initiated by organic peroxides is typically cured by heating the one-part systems containing linear silicone chains and the peroxide catalyst. Peroxides were broken into free radicals, and the free radicals initiate cross-linking reactions between the side chain groups. The curing time of the PDMS depends on the different activation temperatures of different peroxide catalysts.

The second method for curing silicone rubber used a two-part system, with one part containing the Pt cross-linking agent combined with silicone hydride substituted monomers and the other consisting predominantly of methyl vinyl-based silicones, that is mixed just prior to casting. In the presence of platinum catalyst, addition reactions result in a uniformly cross-linked PDMS. The efficiency of the cross-linking reaction is affected by the distance between the hydride groups and the vinyl level of the precursors.

## Introduction

PDMS is ideal for biological applications using aqueous buffers, because PDMS is easily molded, cut and processed into many kinds of functional microfluidic devices. PDMS also has very good elasticity, which makes it ideal for the fabrication of multilayer microfluidics with pumps and valves.

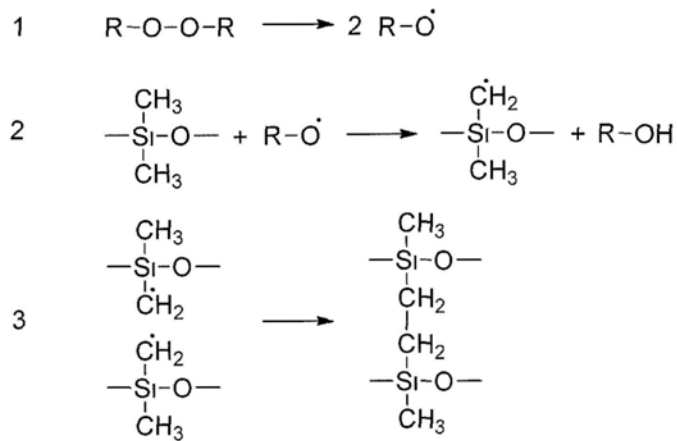


**Figure 1.2** A brief mechanism for peroxide-based PDMS cross-linking.

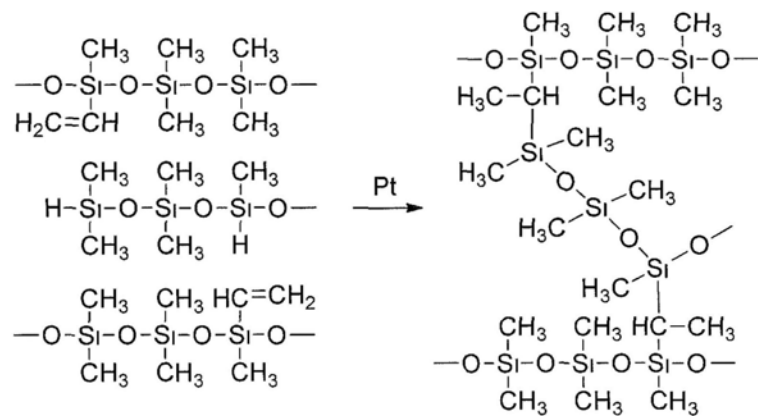


**Figure 1.3** A brief mechanism for platinum-based PDMS cross-linking.

## Introduction

### 1.2.1 Multilayer microfluidics and pneumatic valves

Soft lithography refers to a non-photolithographic strategy based on self-assembly and replica molding for fabricating or replicating structures using elastomeric stamps, molds, and photomasks.<sup>11, 12</sup> It provides an effective, convenient and inexpensive method for the formation and manufacturing of micro- and nanostructures. It is called “soft” because it uses elastomeric materials, such as PDMS. In soft lithography, an elastomeric stamp with patterned relief structures on its surface is used to generate patterns and structures with feature sizes ranging from tens of nanometers to hundreds of microns. A group of soft lithography techniques have been developed, including microcontact printing ( $\mu$ CP),<sup>13</sup> replica molding (REM),<sup>14</sup> microtransfer molding ( $\mu$ TM),<sup>15</sup> micromolding in capillaries (MIMIC),<sup>16</sup> and solvent-assisted micromolding (SAMIM).<sup>17</sup>

Multilayer soft lithography technique that combines soft lithography with the capability to bond multiple patterned layers of elastomer was first developed by Unger et al.<sup>18</sup> Multilayer structures are constructed by bonding layers of elastomer, each of which is separately fabricated by conventional soft lithography method. The bottom layer has an excess of one of the components, say prepolymer, whereas the upper layer has an excess of the other, like curing agent. After baking of the different layers, the upper layer is peeled off its mold and aligned with the lower layer. Because the upper layer and the lower layer have different excesses of one of the two components, there are reactive molecules remaining at the interface between the layers. Further baking makes the two layers to be permanently bonded. The strength of the interface can be as high as

## Introduction

the strength of the bulk PDMS. Additional layers can be added by simply repeating the process.

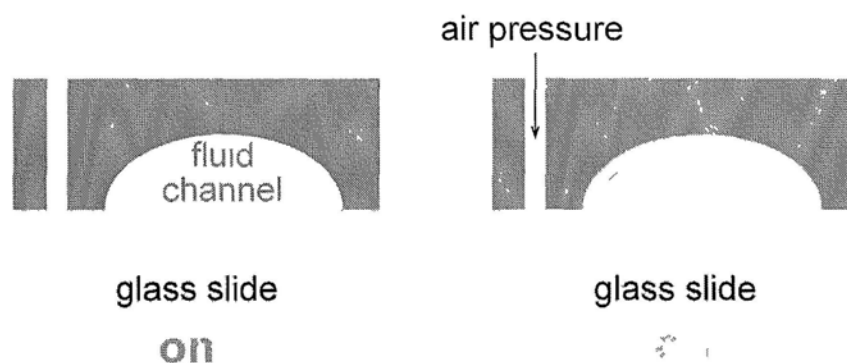


**Figure 1.4** A schematic of pneumatic valves fabricated with PDMS membranes.

To demonstrate the power of multilayer soft lithography, active valves (Figure 1.4) and pumps were fabricated in monolithic elastomeric microfluidic devices.<sup>18</sup> And these valves can be used to make highly integrated chips that are roughly equivalent in their complexity to electronic integrated circuits fabricated with large scale integration.<sup>19</sup> They also can be used in robust manipulation schemes that meter and mix independent of the properties of the working fluid.<sup>20</sup>

### 1.2.2 Droplet-based microfluidic systems

Microdroplets are good carrier for chemical and biological applications because each individual droplet can be ideally considered as a microreactor. A problem in single-phase microfluidic systems is the dispersion of reactants along the microchannels (Figure 1.5). Under hydrodynamic pressure, a parabolic velocity profile is established over the cross-section with fluid velocity zero at the channel walls and maximum at the

## Introduction

channel center.<sup>21</sup> The dispersion of reactants in single-phase microfluidics will usually generate a wide distribution of residence-time of reactants, and will cause significant variation in the reaction kinetics and final product yield.

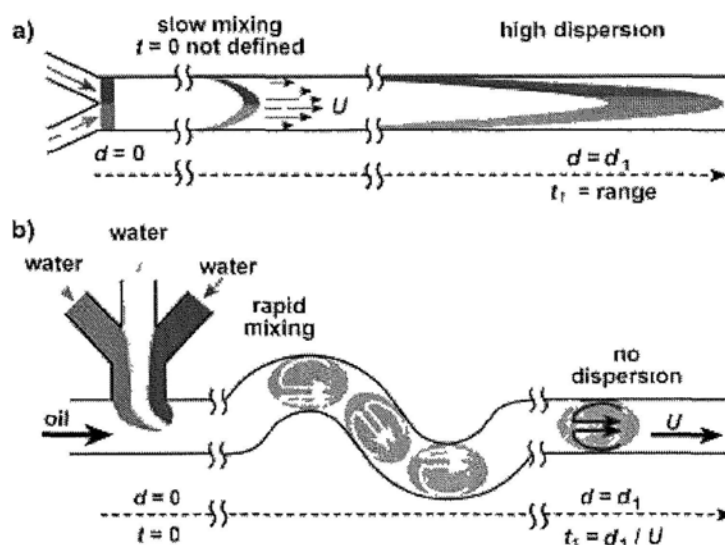


**Figure 1.5** Schematic comparison of a reaction  $A + B$  conducted in a standard pressure-driven microfluidic system device (a) and in droplet-based microfluidic device (b).<sup>22</sup>

Localization of reagents within individual droplets is an effective way of eliminating dispersion. Using droplet system also facilitate precise measurement of reaction times in a microreactor.<sup>22</sup> This precision combination of high droplet throughput and well-defined droplet size makes microdroplet technology an ideal platform for a broad range of in the biomedical sciences, where the enormous diversity of genes, proteins and synthetic molecules has impacted new areas such as combinatorial chemistry, proteomics, genomics, and systems biology. The bottleneck in all these high-

## Introduction

throughput screening technologies is compartmentalization. Microdroplets generated in a rapid and reproducible fashion provide a platform for high-throughput screening.<sup>23-25</sup>

### 1.2.3 Kinetics studies based on microfluidic systems

To solve the problem of large volumes of sample consumption in the conventional kinetics experiments, various microfluidic platforms have been developed. Microfluidics has the advantage of low sample consumption, therefore is an attractive platform for bioanalysis. One of the major difficulties in utilizing microfluidics for bioanalysis, especially for kinetics measurement, is to mix nanoliter of solutions rapidly. Several tricks have been played to enhance mixing in microfluidics.<sup>7, 9, 22, 26</sup> Knight et al.<sup>7</sup> (Figure 1.6a) developed a flow focusing microfluidic device capable of squeezing the central stream to sub-micron in thickness, thus reducing the diffusive mixing times to less than 10  $\mu$ s. The flow focusing device facilitated the study of fast reaction kinetics such as RNA folding on time scales of hundreds of microseconds by monitoring the fluorescence signal in the central stream.<sup>7, 8, 27</sup> Droplet-based microfluidic system is a powerful method for kinetics measurement with advantages such as no dispersion, rapid mixing and on-chip dilution.<sup>9, 22, 28</sup> Song et al.<sup>22</sup> (Figure 1.6b) demonstrated millisecond kinetics measurement on a droplet-based microfluidic chip by moving the droplets through winding microchannels and inducing chaotic flow inside the droplets. Kinetics of the cleavage of a fluorogenic substrate by RNase A was studied by analysis of the fluorescent image of the microfluidic device.

## Introduction

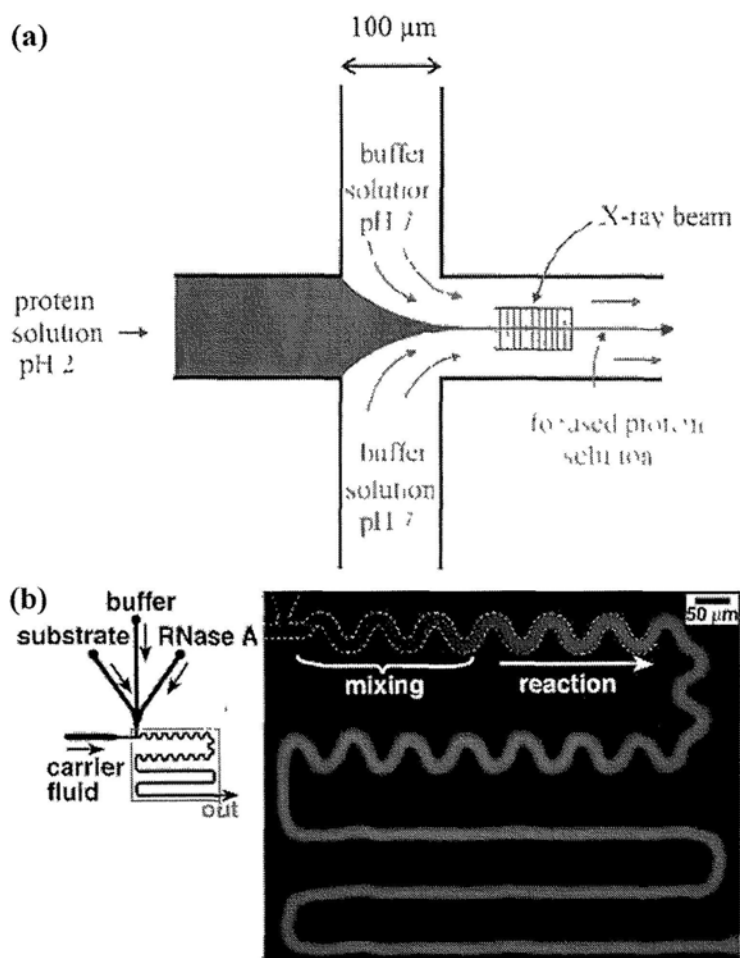


**Figure 1.6** (a) A schematic of the diffusive mixer.<sup>8</sup> (b) Left: a schematic of the microfluidic network. Right: a false-color fluorescence microphotograph.<sup>9</sup>

In both flow focusing and droplet-based microfluidic systems, fluorescence detection is the most widely used detection method, with excellent sensitivity and convenience to implement by using fluorescence microscope. Since most biomolecules have no or extremely weak fluorescence, these molecules need to be labeled with fluorescence tags. The potential issues of using fluorescence tags in kinetics

## **Introduction**

measurement include photo bleaching of the fluorescence tag and interference of the fluorescence tag with the kinetics or function of the target molecules.

## **Introduction**

### **1.3 Electroanalytical detection methods**

Fluorescence microscopy and electrochemistry are two most often used analytical techniques in microfluidics. Electrochemistry detection offers promising applications in microfluidic systems, with features that include simple equipment, portability, low cost, low-power requirements and compatibility with microfabrication technologies.

Electroanalytical techniques are dealing with the relationship between electricity and chemistry. Electroanalysis measures electrical quantities, such as current, potential and their relationship to chemical parameters. Electrical measurements for analytical purpose have a wide range of applications, including biological analysis, environmental monitoring and quality control in industries. There are many kinds of electroanalytical techniques in terms of using different type of electrical signal for the quantitation. The two principal types of electroanalytical measurements are potentiostatic and potentiometric.

#### **1.3.1 Potentiostatic techniques**

Potentiostatic, or controlled-potential techniques deal with the study of charge transfer processes at the electrode / solution interface, and are based on situations with current. Usually the electrode potential is applied to drive an electron transfer reaction and the resultant current is measured. Potentiostatic techniques can thus be applied to measure any chemical species that is electroactive, that is, that can be involved in a redox reaction.

## Introduction

The advantages of potentiostatic techniques include selectivity, a wide linear range, portable and low-cost instrumentation, and a wide range of electrodes that could be used in many applications. Extremely low detection limits ( $\sim 10^{-13}$  to  $10^{-15}$  mol) can be achieved with very small sample volumes. By coupling potentiostatic techniques with chromatographic or optical procedures, sensitivity may be further improved.

### 1.3.2 Potentiometric techniques

Potentiometry is a zero-current technique, in which the concentration or activity about the sample ionic species is measured from the potential established across an ion-selective membrane. Different types of ion-selective membranes have been developed to realize high selectivity. The ion-selective electrodes have thus been widely used for monitoring of ionic species such as  $H^+$ ,  $K^+$ , and  $Ca^{2+}$  ions in complex samples.

Potentiometric techniques are complementary to fluorescence-based techniques in analytical chemistry including kinetics study. The advantages and disadvantages of these two techniques are summarized in table 1.

### 1.3.3 Application of microelectrodes in integrated microfluidics

Electrochemistry offers promising techniques for detection in microchannels with advantages of low cost, tunable selectivity and low-volume sample consumption. The easy miniaturization of electrochemical devices and high compatibility with advanced microfabrication technologies are especially attractive for on-chip applications.

## Introduction

**Table 1** Comparison between ion-selective electrodes and fluorescence labeling

	Advantages	Disadvantages
Ion-selective electrodes	Continuous measurement	Occasionally poor specificity
	Low cost and simple equipment	Electrical interference
	Simple calibration	Response time usually seconds
Fluorescence labeling	Response time of milliseconds	Calibration can be difficult
	Good sensitivities and specificity	Equipment costly
	Continuous measurement	Photo-bleaching, and toxicity

Electrochemical detection has already proven to be extremely useful for capillary electrophoresis (CE) systems.<sup>29-31</sup> The major challenges for such integration are the isolation of the working electrode from the high separation voltage and its proper alignment with the capillary. Additional consideration should be given to the different dimensions, shape, and materials of CE microchips. Woolley et al.<sup>32</sup> reported recently on CE chips with lithographically fabricated electrodes located outside the exit of the channel, Gavin and Ewing<sup>33</sup> developed a thin-film microfabricated electrochemical array detector for planar CE chips, while Wang et al.<sup>29</sup> described an on-chip detector based on sputtering the working electrode directly onto the channel outlet.

A number of works of integrated microfluidic devices have been developed for direct monitoring and detection of various chemicals.<sup>34</sup> Kurita et al.<sup>35</sup> demonstrated a

## Introduction

microfluidic system integrated with dual enzyme-modified microelectrodes for monitoring glucose and lactate *in vivo*. Moser et al.<sup>36</sup> presented a microfluidic chip for measurement of glucose, lactate, glutamine, and glutamate at the same time. A series of thin film platinum working electrodes were fabricated on the glass chip for the measurement. Cai et al.<sup>37</sup> developed a system with integrated microelectrodes that was used for the amperometric detection of lactate *in vivo*. Wu et al.<sup>38</sup> introduced a glucose sensor into a microfluidic system. The sensor contained a separate working electrode that made the fabrication process much easier. These integrated microfluidic devices can measure picoliter samples with concentration as low as picomol. However, the time resolution of the electrochemical detection in these devices was usually at level of several seconds, which is too slow to study rapid kinetics in biological reactions.

# Chapter 2      Measuring rapid enzymatic kinetics by amperometric method in droplet-based microfluidic device

## 2.1 Introduction of enzymatic kinetics and Michaelis-Menten Equation

### 2.1.1 Enzyme kinetics

Enzyme kinetics is the study of the chemical kinetics that are catalyzed by enzymes, which can reveal the catalytic mechanism of the enzyme and its role in metabolism. Enzyme converts substrate(s) to product(s) and accelerates the reaction rate. A unit is the amount of enzyme that will catalyze the conversion of 1  $\mu\text{mol}$  of substrate to product in 1 min under a given set of conditions. An enzyme assay is the act of measuring the reaction velocity, i.e., how fast a given amount of enzyme will convert substrate to product. An enzyme assay requires that the concentration of product and substrate to be determined at a given time after starting the reaction. If the product and substrate have different UV-Vis spectra or fluorescence spectra, the kinetics can be monitored by measuring the change in the spectrum with time. However, it is always the problem to apply UV-Vis spectra in microfluidic system because of the small optical path in microchannels. At the same time, most biomolecules have no or extremely weak fluorescence, these molecules need to be labeled with fluorescence tags. The potential issues of using fluorescence tags in kinetics measurement include photo bleaching of the fluorescence tag and interference of the fluorescence tag with the kinetics or function of the target molecules.

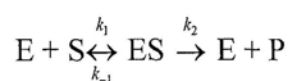
## Rapid Enzymatic Kinetics

Herein we developed a complementary amperometric method based microfluidic system to monitor rapid kinetics in droplets. Many small molecules involved in biochemical reactions, such as metal ions, amino acids and ascorbic acid, can be directly studied by amperometric or other electrochemical methods.

Electrochemical detection methods have great potential in microfluidics because of their low cost, and compatibility with microfabrication technologies. Previously electrochemistry system has been implemented in droplet-based microfluidic system for analysis of equilibrium state concentrations,<sup>39</sup> electroporation of cells,<sup>40, 41</sup> and studying droplets flow behavior.<sup>42</sup> In this chapter, we combine droplets and pneumatic valves in microchannels to control the reaction time, and concentrations at different reaction times are measured by amperometric method. We validate the system by measuring the Michaelis-Menten kinetics of the decomposition of H<sub>2</sub>O<sub>2</sub> by catalase.

### 2.1.2 Michaelis-Menten kinetics

Leonor Michaelis and Maud Menten in 1913 postulated that the enzyme first combines reversibly with the substrate to form an enzyme-substrate complex in a relatively fast and reversibly step. The ES complex then breaks down in a slower step to yield the free enzyme and the product P. At the beginning of the reaction, the concentration of the product, [P], is negligible. The overall reaction can be represented as



## Rapid Enzymatic Kinetics

A key factor affecting the rate of an enzyme reaction is the concentration of the substrate, [S]. As substrate is consumed, the substrate concentration [S] falls and the reaction may get slower. As the product is made, the reaction may slow down if the product is an inhibitor of the enzyme. Some enzymes are unstable and die as you are assaying them. One simple approach in kinetics experiments is to measure the initial velocity,  $V_0$ , when [S] is significantly greater than the concentration of enzyme [E]. Usually [S] may be one million times higher than the [E], and the changes of [S] in the beginning of the reaction can be ignored and considered as a constant. A typical effect on  $V_0$  by varying [S] is shown in Figure 2.1. At low concentration of substrate,  $V_0$  increase linearly with the increasing [S]. At higher concentration of substrate,  $V_0$  gradually reaches to a plateau region, which is close to the maximum velocity,  $V_{\max}$ .

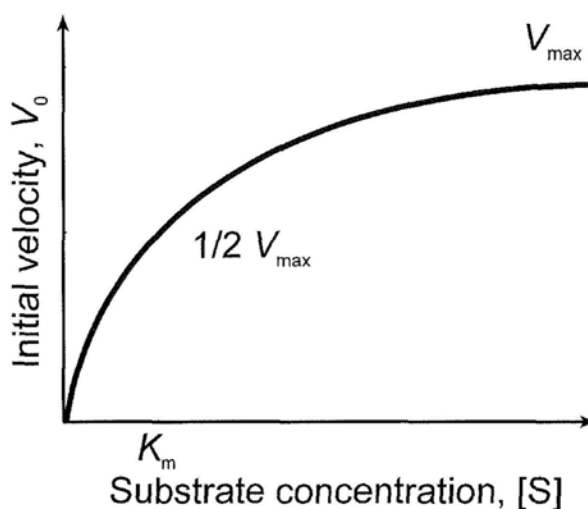


**Figure 2.1** Effect of substrate concentration on the initial velocity of an enzyme-catalyzed reaction.

## Rapid Enzymatic Kinetics

Because the conversion of ES to E and P is relatively slow and is the rate limiting step of the overall reaction, the overall rate is proportional to the concentration of the ES complex.  $V_0$  is determined by the breakdown of ES

$$V_0 = k_2[ES]$$

However [ES] cannot be easily measured experimentally. By introducing total enzyme concentration  $[E_t]$ ,<sup>43</sup> the rates of the formation and breakdown of ES complex can be expressed as

$$[ES] = \frac{[E_t][S]}{[S] + (k_2 + k_{-1})/k_1}$$

The term  $(k_2 + k_{-1})/k_1$  is defined as the Michaelis constant ( $K_m$ ), and the equation could be further simplified to

$$[ES] = \frac{[E_t][S]}{K_m + [S]}$$

When enzyme is saturated,  $[ES] = [E_t]$ , and  $V_{max}$  can be defined as  $k_2[E_t]$ , therefore

$$V_0 = \frac{V_{max}[S]}{K_m + [S]}$$

This equation is called the Michaelis-Menten equation, which is the rate equation for on-substrate enzyme-catalyzed reactions. The equation describes the relationship between the initial velocity  $V_0$ , the maximum velocity  $V_{max}$  and the initial substrate concentration [S] through the Michaelis constant  $K_m$ .

### 2.2 Experimental

#### 2.2.1 Fabrication of microelectrodes

5 mm-long Pt wire (diameter 30  $\mu\text{m}$ , Sino-Platinum Metals) was cut and soldered with a 2 cm-long Ag wire (diameter 150  $\mu\text{m}$ , Sino-Platinum Metals) and was used as Pt working electrode. AgCl was deposited electrochemically on another piece of 3 cm-long Ag wire (diameter 50  $\mu\text{m}$ , Sigma-Aldrich) in 0.15 M NaCl aqueous solution for 1 hour with 0.5 mA current and was used as quasi-reference electrode.

#### 2.2.2 Fabrication of multilayer microfluidics with pneumatic valves

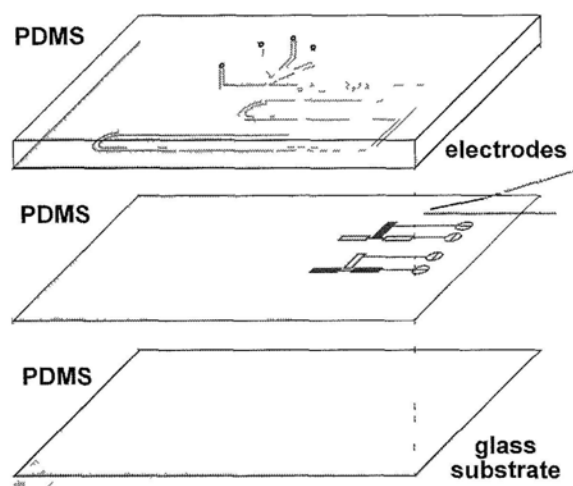


**Figure 2.2** A scheme of the fabrication of multilayer microfluidic devices.

The fabrication of multilayer devices was performed as described previously (Figure 2.2).<sup>10, 18</sup> Master molds for multilayer devices were fabricated by photolithography. Fluid layer mold was made by spin-coating 50  $\mu\text{m}$ -thick positive photoresist (AZ P4620, AZ electronic materials) on silicon wafer and patterning it with a

## Rapid Enzymatic Kinetics

high-resolution photomask. The mold with the patterned photoresist was baked at 110 °C for an hour to transform the cross section of the patterned photoresist to a half-moon geometry that allowed full valve closure.<sup>18</sup> Control layer mold was made by spin-coating and patterning a 25 μm-thick SU-8 photoresist (GM 1060, Gersteltec) on silicon wafer. A degassed 5:1 mixture of a PDMS precursor with the curing agent (Sylgard 184, Dow Corning) was cast as a fluid layer with thickness of 5 mm. A degassed 20:1 mixture of a PDMS precursor with the curing agent was spin-coated at 3000 rpm for 60 s to form a 25 μm-thick control layer. Both fluid and control layers were first cured for 30 min at 80 °C and then the fluid layer was aligned and sealed on the control layer to form the microchannels for the fluid layer. Bonding between these two layers was accomplished by curing the devices for another 60 min at 80 °C. The combined PDMS piece was then bound to a flat piece of PDMS substrate to form the microchannels for the control layer (Figure 2.3a). Pt and Ag/AgCl microelectrodes were inserted into the microchannel in the fluid layer and sealed with epoxy glue (inset of Figure 2.3b).

## Rapid Enzymatic Kinetics

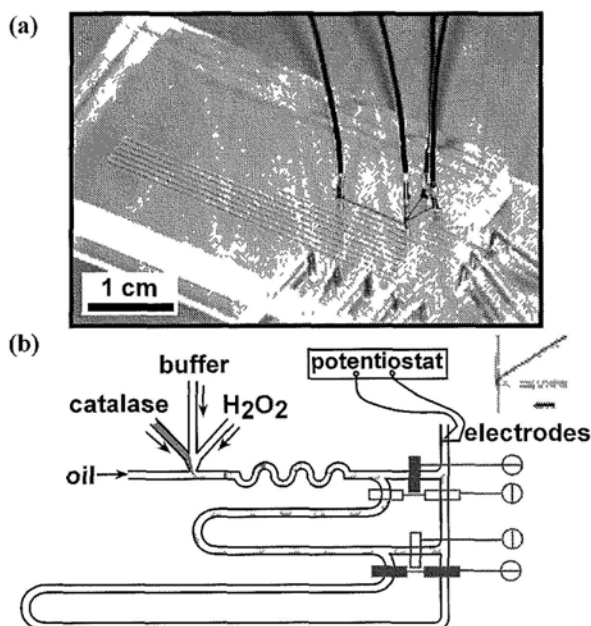


**Figure 2.3** Multilayer microfluidics for enzymatic kinetics experiments. (a) Photograph of the multilayer PDMS device. (b) Scheme of multi-time range access controlled by pneumatic valves (in purple) in a multilayer microfluidic device. Inset is the microphotograph of microelectrodes inserted near the outlet of the microchannel. Scale bar is 500  $\mu\text{m}$ .

### 2.2.3 Sample preparation and operation

Catalase (from bovine liver, 2000-5000 units/mg, Sigma) was dissolved in 50 mM phosphate buffered saline (PBS, pH 7.4) at 10.0  $\mu\text{g/ml}$ . Hydrogen peroxide (33%, Panreac) was diluted by 50 mM PBS buffer to 200 mM. Precision syringe pumps (PHD 2000, Harvard Apparatus) were used to drive the flow of catalase solution, the diluting buffer, and the carrier fluid. Teflon tubing (Stranco) was used to connect syringes with microfluidic channels. Silicon oil (viscosity 50 cp, Brookfield) was used as the carrier

## Rapid Enzymatic Kinetics

fluid, and droplets containing the mixture of PBS buffer, substrate solution and catalase solution were formed at the junction (Figure 2.3b).

Each control channel for the pneumatic valves was connected to a homemade three-way switch through Tygon tubing (Cole-Parmer). Regulated compressed air (0.2 MPa) was applied to the three-way switch, and control channel can be pressured or vented to atmosphere by controlling the three-way switch.

The Pt and Ag/AgCl microelectrodes were separately connected to a potentiostat (263A, Princeton Applied Research) for electrochemical analysis of the droplets in the microchannel (Figure 2.3b).

Microphotographs were taken by using a stereoscope (MZ 16, Leica) equipped with a CCD camera (SPOT Insight, Diagnostic Instruments). A Machine Vision Strobe X-Strobe X1200 (Perkin-Elmer Optoelectronics) provided lighting. The flash duration of the strobe light was  $\sim 10 \mu\text{s}$ .

## Rapid Enzymatic Kinetics

### 2.3 Results and discussion

#### 2.3.1 Control of reaction time in droplets

The reaction started once the droplets were generated by combining the aqueous streams and injecting them into the flow of silicone oil at the junction of the microchannel (Figure 2.3b). The reaction time in the droplets was the time that the droplets spent in the microchannel until they arrived at the microelectrodes. There were two ways to vary the reaction time in the droplets in our microfluidic system: (1) changing the flow rate to tune the reaction time; (2) using the pneumatic valves to change the flow route and in turn the travel time of the droplets (Figure 2.4).

When the flow rate was varied to tune the reaction time, the maximum flow rate was limited by the highest pressure allowed at the inlets of the PDMS device. On the other hand, low flow rate led to long droplets, which required long mixing time as the droplets flowed through the winding microchannel.<sup>44</sup> In our experiment, the flow rate varied between 10 mm/s and 100 mm/s. Since most reactions are of positive reaction order, it is necessary to obtain more data points in the initial stage of the reactions in the kinetics measurement. We varied the flow rates when the droplets moved in the shortest route (Figure 2.4a), and the reaction time ranged from 0.05 s to 0.5 s. When the pneumatic valves were used to vary the reaction time in the droplets, the flow rate of the droplets was maintained constant at 10 mm/s. As a result, the combined reaction time ranged from 0.05 s (in the shortest route) to 25 s (in the longest route).

## Rapid Enzymatic Kinetics

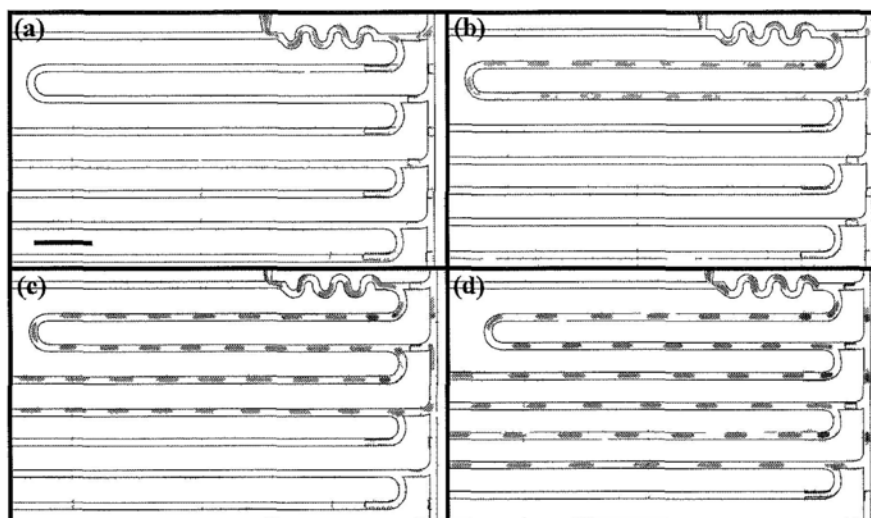


**Figure 2.4** Microphotograph of the droplets moving along different routes controlled by pneumatic valves. (a) Droplets taking the shortest route of  $\sim 5$  mm-long; (b) Droplets taking the second route of  $\sim 20$  mm-long; (c) Droplets taking the third route of  $\sim 50$  mm-long; (d) Droplets taking the fourth route of  $\sim 110$  mm-long. The droplets contained  $\text{Fe}(\text{SCN})_x^{(3-x)+}$  for better observation. The length of droplets was shorter at the position where a valve was located, because the flexible PDMS membrane between the fluid channel and valve was forced to go down, increasing the height of the fluid channel.

### 2.3.2 Rapid mixing

The time resolution of the current device is 0.05 s, which is limited by the maximum total flow rate  $v_{\text{max}}$  (100 mm/s) and the distance between the T-junction for droplets formation and the microelectrodes (5 mm). The segment of winding channel induced chaotic advection inside the droplets, which led to rapid mixing of the reagents in each droplet.<sup>9</sup> It has been shown that efficient mixing can be achieved by driving the droplets through only a short segment of such winding channel.<sup>28</sup> We used pyranine to

## **Rapid Enzymatic Kinetics**

characterize the mixing time in our droplet-based microfluidic system. Fluorescence intensity of pyranine increased dramatically when the solution pH changed from acidic to basic. By monitoring the fluorescence change of the droplets containing acidic pyranine solution (0.5 mM, pH ~ 1) and NaOH solution (pH ~ 14), we found that the mixing was completed within 0.02 s in our experiment (Figure 2.5), which was shorter than the time resolution of the device.

## Rapid Enzymatic Kinetics

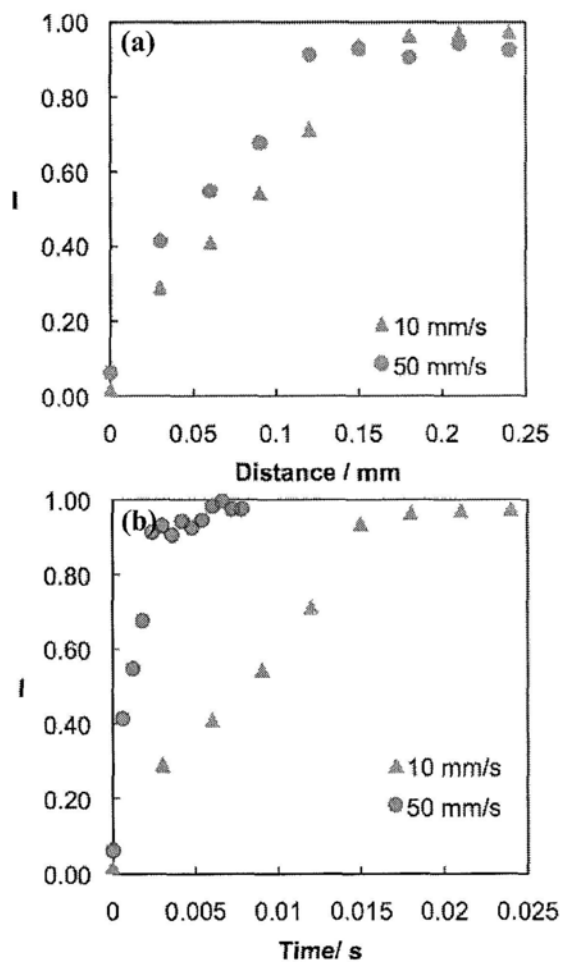


**Figure 2.5** Rapid mixing was achieved with winding channels. Normalized fluorescence intensity ( $I$ ) obtained from microphotograph (2 s exposures) as a function of the travel distance (a) and as a function of travel time (b) of the droplets at two different flow rates. Fluorescence intensity increased when acidic pyranine solution (0.5 mM, pH  $\sim$  1) mixed with NaOH solution (pH  $\sim$  14) inside of droplets. The average intensity across the width of the microchannel was measured.

## Rapid Enzymatic Kinetics

### 2.3.3 Electrochemistry of hydrogen peroxide in microchannels

H<sub>2</sub>O<sub>2</sub> is oxidized at the surface of metal electrodes such as platinum polarized to 600 mV:<sup>45</sup>



In our microfluidic system, the aqueous droplets containing H<sub>2</sub>O<sub>2</sub> and the carrier fluid alternatively passed by the microelectrodes, and the electrochemical circuit was connected and disconnected, resulting in a periodic current rise and fall (Figure 2.6). The peak value was stable and reproducible, with a CV of 5%. The occurrence of each current peak signal can be divided into three stages (Figure 2.7): (1) the aqueous droplet approached the two microelectrodes, and became in contact with only the first microelectrode (Figure 2.7b); (2) the droplet moved further along the channel, and became in contact with both microelectrodes, and a current peak was generated (Figure 2.7c); (3) the droplet was disconnected from the first microelectrode, the current signal returned to zero (Figure 2.7d). To make a complete electric circuit, the droplet must be longer than the gap between the two microelectrodes. In the microfluidic device, the two microelectrodes were placed with a gap smaller than the cross-sectional dimension of the microchannel. In our experiments, the capillary number ( $Ca = \mu v / \gamma$ , where  $\mu$  is viscosity,  $v$  is the flow velocity of carrier fluid, and  $\gamma$  is interfacial tension) was less than 0.005, and the width of the main channel was comparable to the width of the aqueous inlet (Figure 2.4). Under these experimental conditions, the droplets formed in the microchannel were in the form of “plugs”,<sup>46, 47</sup> with the length longer than the cross-sectional dimension of the microchannel and the microelectrodes gap, ensuring that the

## Rapid Enzymatic Kinetics

electrochemical circuit was always completed when a droplet passed by the microelectrodes. As long as the length of droplets was longer than the gap between the microelectrodes, the current signals were stable and reproducible, with a CV of 5%.

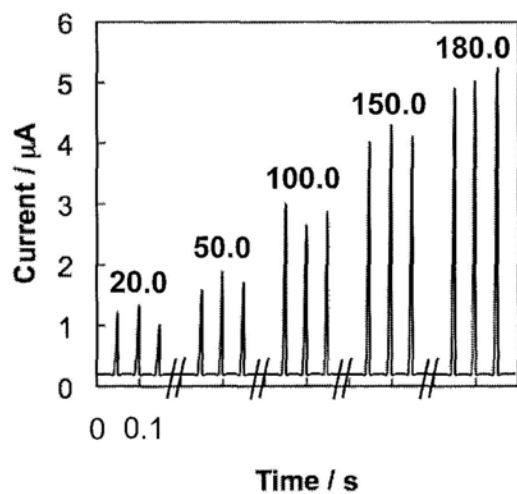


**Figure 2.6** Current profile measured at 0.6 V (vs. Ag/AgCl quasi-reference electrode) for H<sub>2</sub>O<sub>2</sub> concentration ranging from 10 mM to 200 mM. Numbers on top of each group of peaks indicate the concentrations of H<sub>2</sub>O<sub>2</sub> in mM. The lowest concentration of H<sub>2</sub>O<sub>2</sub> used in the experiment was 6.67 mM, however the detection limit of amperometric method can be as low as nanomolar.

## Rapid Enzymatic Kinetics

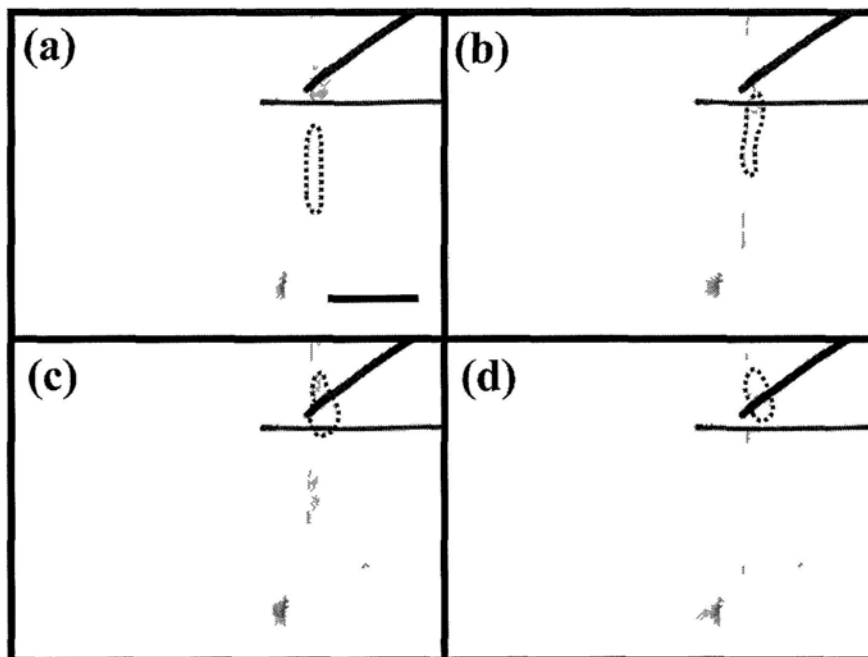


**Figure 2.7** A serial of microphotographs showing droplets passing through the two microelectrodes. The droplets contained  $\text{Fe}(\text{SCN})_x^{(3-x)+}$  for better observation. One droplet was highlighted by dashed line. (a) The highlighted droplet was approaching the microelectrodes; (b) The droplet just contacted the first microelectrode, Pt electrode; (c) The droplet moved further to connect both microelectrodes and a current signal was generated; (d) The droplet disconnected with the first microelectrode and current returned to zero.

We noticed that some droplets were split after the droplets passed the Ag/AgCl quasi-electrode (Figure 2.7). Although the splitting did not interfere with the electrochemical measurement, it would be desirable to control the splitting event in case more studies of the droplet content were required after the electrochemical measurement. We found that the splitting can be avoided by using smaller-sized microelectrodes

## Rapid Enzymatic Kinetics

(Figure 2.8). In addition, reducing the length of the microelectrodes presented in the microchannel might also help prevent the splitting of the droplets (Figure 2.9).

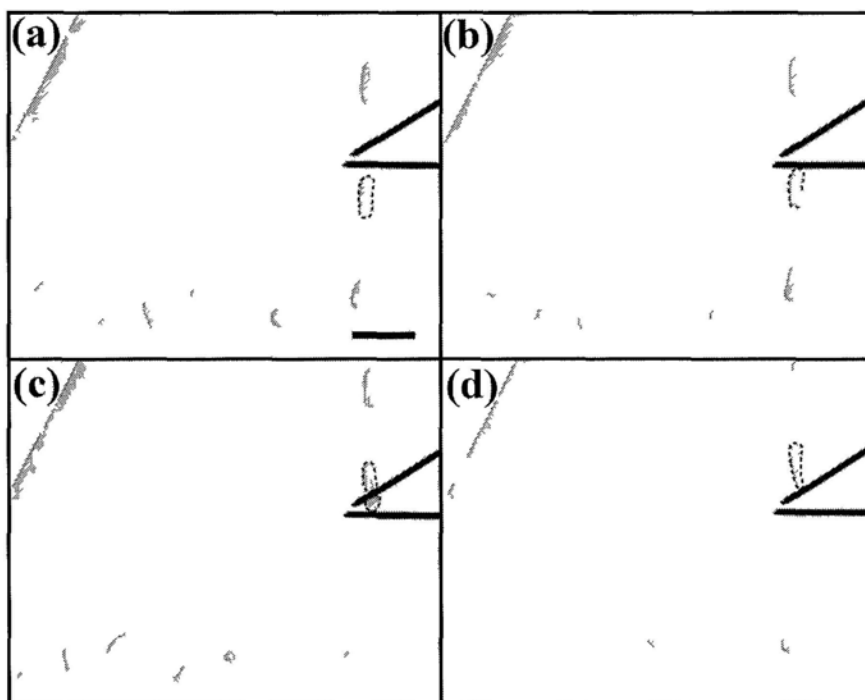


**Figure 2.8** A series of microphotographs showing droplets passing by the two stainless steel wires (diameter  $\sim 20 \mu\text{m}$ ), which were extended laterally across the microchannel. The droplets contained  $\text{Fe}(\text{SCN})_x^{(3-x)+}$  for better observation. One droplet was highlighted by dashed line. (a) The highlighted droplet was approaching the metal wires; (b) The droplet just contacted the first metal wire; (c) The droplet moved further to connect both metal wires; (d) The droplet disconnected with the first metal wire. Scale bar is  $500 \mu\text{m}$ .

## Rapid Enzymatic Kinetics

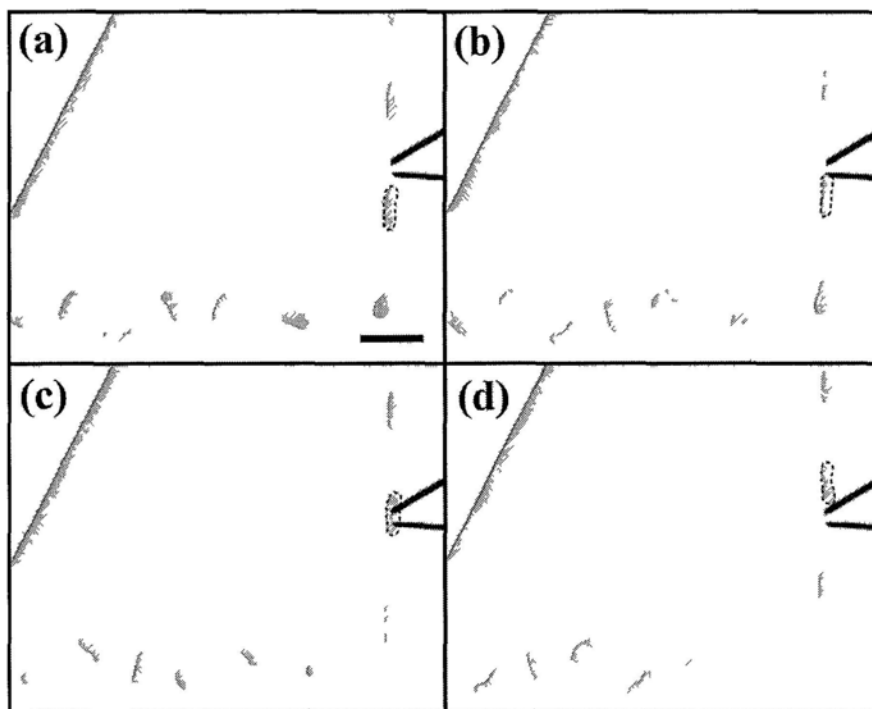


**Figure 2.9** A series of microphotographs showing droplets passing by the two stainless steel wires (diameter  $\sim 20 \mu\text{m}$ ), which were extended laterally to only the middle of the microchannel. The droplets contained  $\text{Fe}(\text{SCN})_x^{(3-x)+}$  for better observation. One droplet was highlighted by dashed line. (a) The highlighted droplet was approaching the metal wires; (b) The droplet just contacted the first metal wire; (c) The droplet moved further to connect both metal wires; (d) The droplet disconnected with the first metal wire. Scale bar is  $500 \mu\text{m}$ .

In our electrochemical detection setup, we found that the current peak was independent on the flow rate of the droplets (Figure 2.10b), indicating that diffusion was not the limiting step in the electrochemical oxidation of  $\text{H}_2\text{O}_2$ . Our observation was consistent with previous studies on the electrode reaction of  $\text{H}_2\text{O}_2$ ,<sup>48-51</sup> which found the

## **Rapid Enzymatic Kinetics**

reaction to be irreversible and sensitive to the surface roughness of the electrode. The quantitative treatments of the flow and of the response of the hydrodynamic microelectrode in the microchannel are beyond the scope of the current work, and the complete understanding of the mechanism of the electrochemical response in our two-phase system requires further study.

## Rapid Enzymatic Kinetics

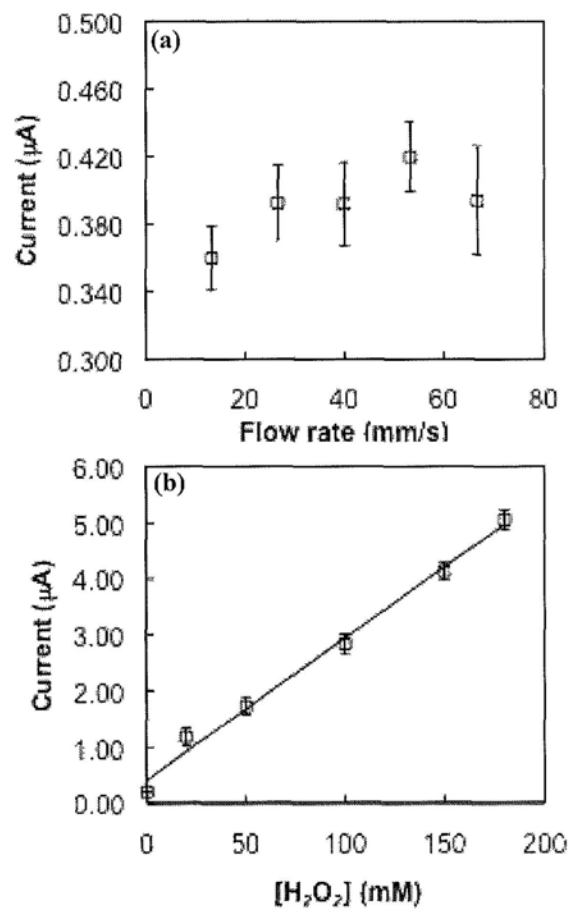


**Figure 2.10** Calibration of microelectrodes with different flow rates and  $\text{H}_2\text{O}_2$  concentrations. (a) Calibration curve for  $\text{H}_2\text{O}_2$  concentration ranging from 10 mM to 200 mM with the linear fitting of the experimental data. (b) Relationship between current and flow rate of the droplets. The concentration of  $\text{H}_2\text{O}_2$  was 50 mM and the flow rates were from  $\sim 10$  mm/s to  $\sim 70$  mm/s.

### 2.3.4 Analysis of the enzymatic kinetics

The current amplitude in the electrochemical system depends on two factors: (1) the bulk concentration of the analyte; (2) the flow rate of the droplets when diffusion is a

## Rapid Enzymatic Kinetics

limiting factor in the electrochemical reaction. Accordingly two calibration curves would be required for using amperometric method to analyze the droplet content in the current microfluidic system: (1) the current signal dependence on the concentration of the electrochemically active molecule; (2) the current signal dependence on the flow rate of the droplets. Both calibration curves could be obtained in a single experimental run by manipulating the individual flow rates of  $\text{H}_2\text{O}_2$  stream, the diluting buffer stream, and the carrier fluid. The first calibration curve (Figure 2.10a) was established at varying concentration of  $\text{H}_2\text{O}_2$  in the droplets by changing the ratio of the flow rates of the buffer and  $\text{H}_2\text{O}_2$  streams while maintaining the combined flow rate constant. In the concentration range in our experiment for enzyme activity measurement, the peak heights of the current signal were linearly proportional to the concentration of  $\text{H}_2\text{O}_2$  in the droplets. The second calibration curve was established by gradually increasing the flow rates of both  $\text{H}_2\text{O}_2$  solution and the buffer, while the ratio of the two aqueous streams was maintained constant (Figure 2.10b). As we mentioned in the previous section, the current signal of  $\text{H}_2\text{O}_2$  oxidation was independent of the flow rate, therefore the second calibration curve was essentially a flat line in the case of electrochemical oxidation of  $\text{H}_2\text{O}_2$ . As a result, the analysis of the current signal of  $\text{H}_2\text{O}_2$  oxidation was simplified by referring to only the calibration curve of the current versus the bulk concentration of  $\text{H}_2\text{O}_2$ .

The calibration of the current signal versus  $\text{H}_2\text{O}_2$  concentration was performed both before and after the Selwyn's test (Figure 2.11). The two superimposable

## Rapid Enzymatic Kinetics

calibration curves suggested that there was no obvious adsorption of protein or other contaminants on the surface of the microelectrodes (Figure 2.12).

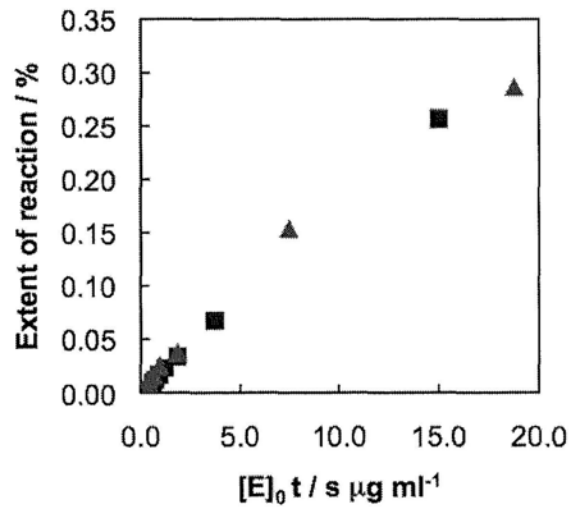


**Figure 2.11** The Selwyn plot for catalase.  $\text{H}_2\text{O}_2$  concentration was 66.7 mM. Two catalase concentrations, 5  $\mu\text{g}/\text{ml}$  (red triangles) and 10  $\mu\text{g}/\text{ml}$  (blue squares), were tested.

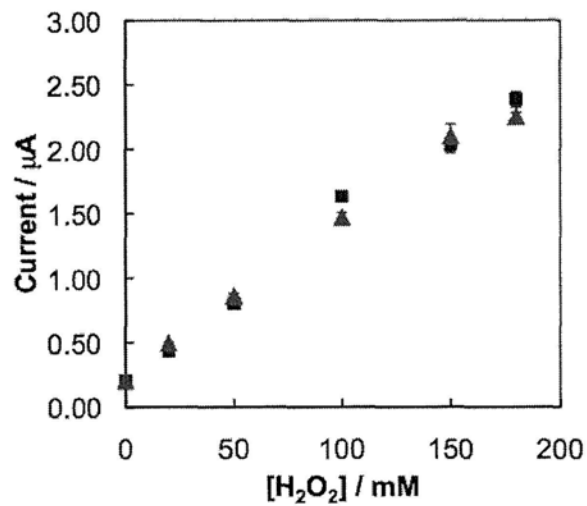


**Figure 2.12** Calibration curves of the current versus  $\text{H}_2\text{O}_2$  concentration before (blue squares) and after Selwyn's test (red triangles).

## Rapid Enzymatic Kinetics

The reaction kinetics was analyzed following the typical Michaelis-Menten kinetics. The Michaelis-Menten kinetics does not always apply to the decomposition of  $\text{H}_2\text{O}_2$  by catalase because of the two-step nature of the catalytic reaction.<sup>52</sup> However, in our experiment with  $\text{H}_2\text{O}_2$  concentration below 200 mM, catalase does exhibit a Michaelis-Menten kinetics.<sup>53</sup> In a single-run experiment, we obtained multiple reaction kinetics at different starting  $\text{H}_2\text{O}_2$  concentration and constant catalase concentration (Figure 2.13a). Each curve in Figure 2.13a was composed of two segments. The first segment was from 0.05 s to 0.5 s and was obtained by changing the flow rate of the droplets in the shortest route (inset of Figure 2.13a). The second segment was from 1.5 s to 8.0 s and was obtained by using the pneumatic valves to change the flow routes of the droplets. The initial velocities ( $V$ ) of the enzymatic reaction were calculated at different concentration of  $\text{H}_2\text{O}_2$  from the linear portion of the kinetics curves in the initial stage of the reaction. By plotting initial velocities versus different concentrations of  $\text{H}_2\text{O}_2$  at the same catalase concentration, a Michaelis-Menten kinetics curve was obtained (Figure 2.14). The Michaelis constant  $K_m$  and the maximum velocity  $V_{max}$  were calculated as 62 mM and 22 mM/s by plotting  $V^{-1}$  against  $[\text{H}_2\text{O}_2]^{-1}$  (Figure 2.13b). These values were consistent with previous measurements of bovine catalase under similar experimental conditions, where  $K_m$  ranged from 64 mM to 537 mM.<sup>53</sup>

## Rapid Enzymatic Kinetics

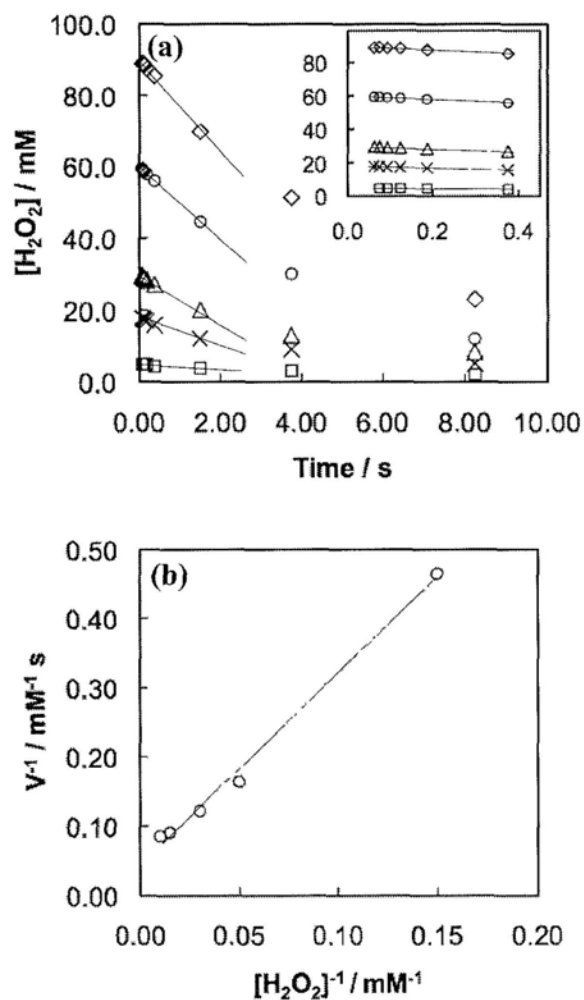


**Figure 2.13** Plots for Michaelis-Menten kinetics analysis. (a) Plot of  $\text{H}_2\text{O}_2$  vs. the reaction time. The starting  $\text{H}_2\text{O}_2$  concentrations are 100 mM (“ $\diamond$ ”), 66.7 mM (“ $\circ$ ”), 33.3 mM (“ $\Delta$ ”), 20.0 mM (“ $\times$ ”), and 6.67 mM (“ $\square$ ”), respectively. Inset is the blow-up of the plot in the time range from 0 to 0.5 s. (b) Plot of  $V^{-1}$  vs.  $[\text{H}_2\text{O}_2]^{-1}$  for Michaelis-Menten kinetics analysis. Kinetics was measured three times for each different starting  $\text{H}_2\text{O}_2$  concentration.

## Rapid Enzymatic Kinetics

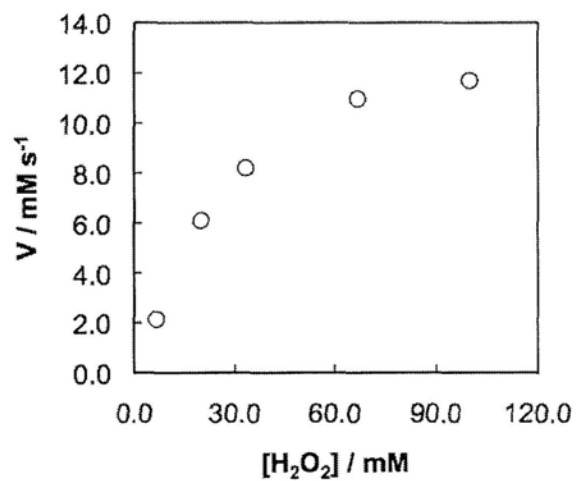


**Figure 2.14** Plot of initial velocity ( $V$ ) vs. different substrate concentrations ( $[H_2O_2]$ ) at the same catalase concentration ( $10 \mu\text{g/mL}$ ).

## Rapid Enzymatic Kinetics

### 2.4 Conclusions

We integrated the electrochemical detection method into a droplet-based microfluidic system for measuring rapid kinetics. Pneumatic valves were implemented to control the reaction time. In this work, the best time resolution was about 0.05 s. A complete Michaelis-Menten kinetics measurement with five different H<sub>2</sub>O<sub>2</sub> concentrations was achieved in a single experimental run, and the total consumption of samples was less than 50  $\mu$ L.

This microfluidic system is complementary to the fluorescence-based microfluidic system. Only one pair of microelectrodes was employed in the microfluidic system, making the PDMS chip simple and inexpensive to fabricate, and the chip can be disposable. It is possible to further simplify the fabrication of the chip by separating the microelectrodes from the microfluidic channels.<sup>29</sup> The current microfluidic system is applicable to many biochemical reactions, as long as one of the reactants or products is electrochemically active. With appropriate quenching method at the outlet, the reaction in the droplets can be “frozen” at different reaction times, allowing the droplets to be analyzed offline, for example by mass spectrometry.<sup>54</sup> In this way various detection methods can be integrated into the microfluidic system, further extending the application of the combination of pneumatic valves and droplets in microchannels.

### Chapter 3      Measuring RNA-Mg<sup>2+</sup> binding kinetics by potentiometric method in droplet-based microfluidic device

#### 3.1 Introduction of Mg<sup>2+</sup> induced RNA folding and its kinetics

##### 3.1.1 The concept of ion binding

The strong attractive interactions between cations and RNAs are usually described by the formation of different binding states in solution.<sup>55</sup> Similar with protein solutions,<sup>56</sup> the binding states in RNAs are often classified as two different types, diffusely binding and site binding, depending on the strength of their interaction with the RNAs (Figure 3.1).<sup>57</sup>

In diffuse binding, cations interact with the strong anionic field around the nucleic acid backbone through nonspecific long-range electrostatic interactions.<sup>58</sup> As a result, the hydration shells of the ions and the RNA remain intact of this relatively weak interaction between the cations and the RNA (Figure 3.1a).

In site binding, the thermal translational energy of ions are not sufficient to overcome the relatively strong local attractive forces and trapped near the surface of the RNA.<sup>56</sup> Ions can be localized on the surface of the RNA in two different ways (Figure 3.1b and c).<sup>59</sup> The first type of site binding is also termed an “outer-sphere” complex.<sup>60</sup> The strong electrostatic field surrounding nucleic acids results in the accumulation of cations in pockets of negative electrostatic potential created by the irregular shape of the molecular surface (Figure 3.1b).<sup>61-64</sup> In the second type of site binding, an ion strongly

## RNA-Mg<sup>2+</sup> Binding Kinetics

interacts with the RNA by directly contacting a set of RNA ligands with no water molecules (Figure 3.1c). Such type of site binding is sometimes called an “inner sphere” complex, like the corresponding state for a divalent metal ion and a sulfate anion.<sup>65</sup>

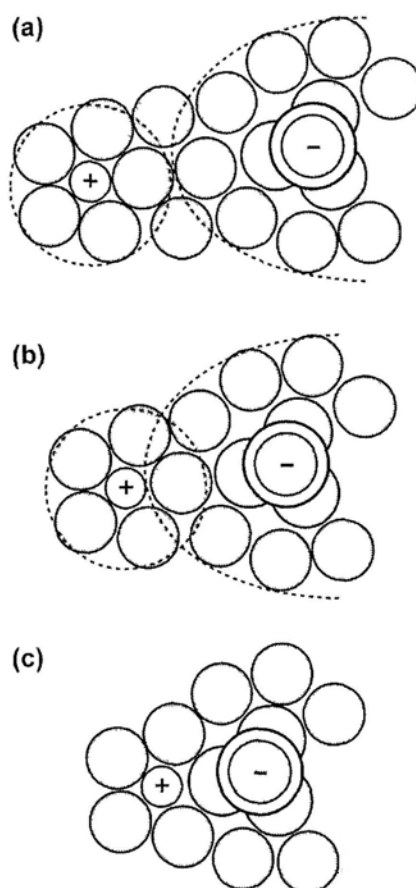


**Figure 3.1** Modes of ion binding to RNA. (a) Diffuse binding in which the solvation shell (dotted line) of the ion and its phosphate ligand remain intact. (b) Outer sphere complex in which the ion and its ligand share their solvation shells. (c) Inner sphere complex in which the ion and its ligand make direct contact without intervening waters. Mg ion is green. Water molecules are blue. Phosphorous atom is yellow and oxygen atoms are red.

## RNA-Mg<sup>2+</sup> Binding Kinetics

### 3.1.2 *Tetrahymena* group I ribozyme

Recently, ribozymes derived from the self-splicing *Tetrahymena thermophila* have become a model to understand the effects of Mg<sup>2+</sup> during the Mg<sup>2+</sup>-RNA binding kinetics.<sup>66, 67</sup> The folding kinetics of *Tetrahymena* group I ribozyme has been fully studied using free radical cleavage of ribose to map solvent accessibility of the RNA backbone as a function of Mg<sup>2+</sup> concentration.<sup>66, 68</sup> The experiment results show that the ribozyme folds as two separate but coupled transitions with different Mg<sup>2+</sup> requirements (Figure 3.2).<sup>68</sup> The first transition involves the independent folding of the 160 nucleotide P4–P6 domain coupled to strong Mg<sup>2+</sup> binding ([Mg]<sub>1/2</sub> = 0.7 mM). The remainder of the catalytic core, the P1–P2.1/P3–P9 domain, folds in the second transition with slightly weaker Mg<sup>2+</sup> binding ([Mg]<sub>1/2</sub> = 0.85 mM). The second transition depends strongly on the presence of the intact, folded P4–P6 domain. Therefore, Mg<sup>2+</sup> is important in the thermodynamic stabilization of the RNA, and at the same time, Mg<sup>2+</sup> also influence the kinetic pathways involved in the folding procedures by stabilizing RNA domains differentially.

## RNA-Mg<sup>2+</sup> Binding Kinetics

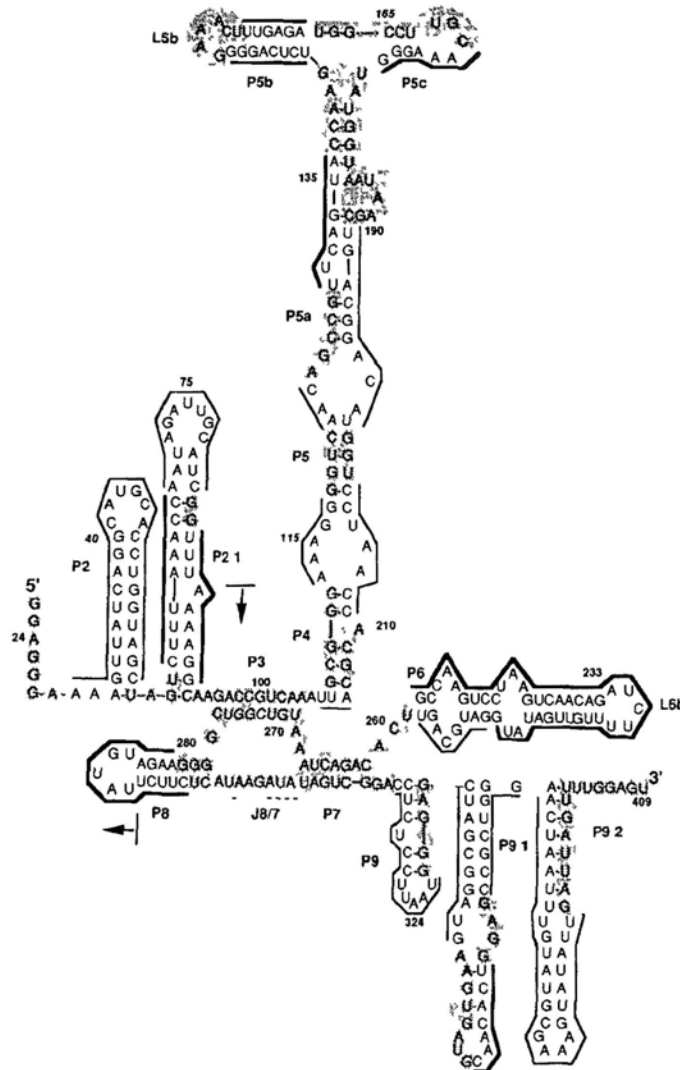


**Figure 3.2** *Tetrahymena* group I ribozyme secondary structures.<sup>66</sup>

The rapid binding kinetics between P4-P6 domain of the *Tetrahymena* group I ribozyme and Mg<sup>2+</sup> falls into the detection range of our droplet-based microfluidic systems. To validate the potentiometric detection method, we integrated Mg<sup>2+</sup>-selective electrode with droplet-based microfluidics and studied the RNA-Mg<sup>2+</sup> binding kinetics.

### 3.2 Experimental

#### 3.2.1 Preparation of Mg<sup>2+</sup> ion-selective electrode

The solid-contact Mg<sup>2+</sup> ion-selective microelectrode (ISE) was prepared by using 5 mm long Pt wires (diameter ~ 30 μm) as solid substrates. The Pt wire was soldered to Ag wires for electric contact. To prepare the Mg<sup>2+</sup> ISE, The Pt wire was first dipped into poly(3-octylthiophene-2,5-diyl) (POT) solution for five seconds and then dried in the air for 15 minutes. This process was repeated for three times. Next the Pt wire with POT coating was treated with Mg<sup>2+</sup> ionophore VI cocktail (Sigma-Aldrich) by dipping the Pt wire into Mg<sup>2+</sup> ionophore VI cocktail for five seconds and then drying the Pt wire in the air for 15 minutes (Figure 3.3). The process was repeated for three times to produce the Mg<sup>2+</sup> ISE. The Mg<sup>2+</sup> ISE was then conditioned in 10<sup>-6</sup> M MgCl<sub>2</sub> for 1 day. The detection limit of the Mg<sup>2+</sup> ISE in the current work was 10 μM. To prepare the reference electrode, AgCl was deposited electrochemically on a 3 cm-long Ag wire (diameter 50 μm, Sigma-Aldrich) in 0.15 M NaCl aqueous solution for 1 h with 0.5 mA current.

## RNA-Mg<sup>2+</sup> Binding Kinetics

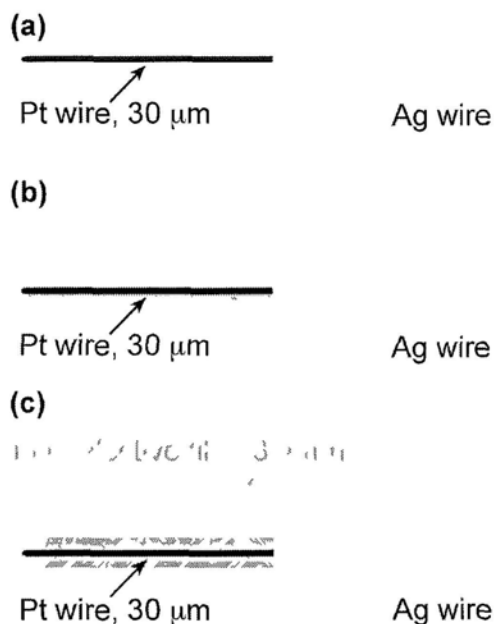


**Figure 3.3** A scheme of the fabrication of solid-contact ion-selective microelectrode.

### 3.2.2. Fabrication of the Microfluidic Devices

The fabrication was performed by soft lithography as described previously (Figure 3.4) and please refer to the appendix A for detailed information.<sup>10, 18</sup> Briefly, two master molds of fluid layer and control layer respectively were fabricated by photolithography. The fluid layer mold was made with positive photoresist (AZ P4620, AZ electronic materials) on silicon wafer and was treated at 110 °C for an hour to form channels with cross section of half-moon geometry. The half-moon geometry facilitated full valve closure. The control layer mold was made by SU-8 photoresist (GM 1060, Gersteltec) on silicon wafer also by photolithography.

Two different ratios of degassed polydimethylsiloxane (PDMS) base and curing agent (Sylgard 184, Dow Corning) mixtures were prepared. 5:1 mixture was cast as a

## RNA-Mg<sup>2+</sup> Binding Kinetics

fluid layer with thickness of 5 mm, and 20:1 mixture was spin-coated at 3000 rpm for 60 s to form a 25 μm-thick control layer. Both fluid and control layers were first cured for 30 min at 80 °C and then aligned and sealed to form the microchannels for another 60 min at 80 °C. Finally, multilayer devices were made by binding fluid and control layers to a flat PDMS slab. The Mg<sup>2+</sup> selective microelectrode and Ag/AgCl microelectrodes were inserted into the microchannels in the fluid layer and sealed with epoxy glue (Figure 3.4).

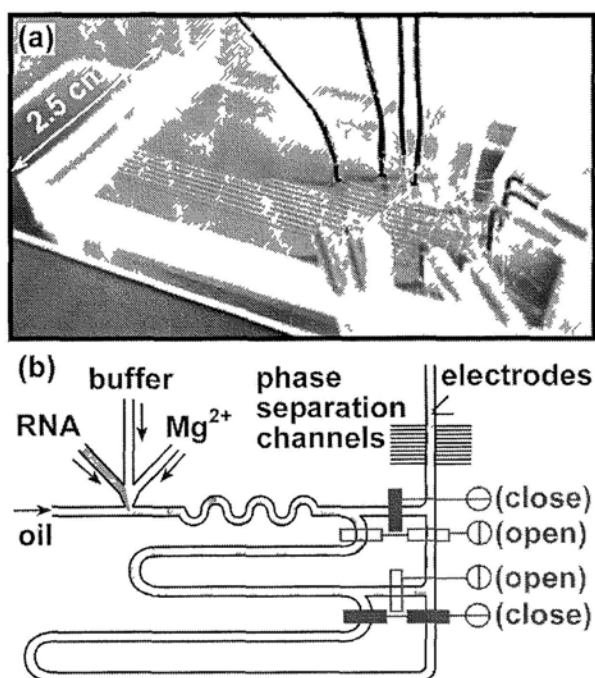


**Figure 3.4** Multilayer microfluidics for RNA-Mg<sup>2+</sup> binding kinetics experiments. (a) Photograph of the multilayer PDMS device. (b) Scheme of multilayer microfluidic device. The movement of droplets is controlled by the pneumatic valves (purple).

## RNA-Mg<sup>2+</sup> Binding Kinetics

### 3.2.3 Preparation of P4-P6 domain of the *Tetrahymena* group I ribozyme

P4-P6 domain of the *Tetrahymena* group I ribozyme constructs were prepared by *in vitro* transcription from PCR-generated DNA templates (TaKaRa, Dalian) using T7 RNA polymerase (please refer to the appendix B).<sup>69</sup> Briefly, *E. coli* competent cell JM109 (TaKaRa, Dalian) was used for transformation. Plasmid was first purified by QIAGEN midi preparation kit (QIAGEN) and then linearized by Not I restriction enzyme (TaKaRa, Dalian). RNA transcription and purification were done by MEGashortscript and MEGAclean kit (Applied Biosystems). About 100 µg purified RNA could be obtained for each kit reaction and different concentrations was prepared for RNA-Mg<sup>2+</sup> binding kinetics experiment.

### 3.2.4 Instrumentation for the potentiometric measurements

Pneumatic valves in control layer were connected to and controlled by a homemade three-way switch through Tygon tubing (Cole-Parmer).

Microphotographs were taken by a stereoscope (MZ 16, Leica) equipped with either a CCD camera (SPOT Insight, Diagnostic Instruments) or a high speed camera (FASTCAM 1024PCI, Photron).

A multifunction data acquisition (DAQ) board (NI USB-6216, National Instruments) connected with a homemade high impedance interface was used for potentiometric measurements.

### 3.3 Results and discussion

#### 3.3.1 Integration of Mg<sup>2+</sup> selective microelectrode in microfluidic devices

To measure the content of the droplets by electrochemical methods, the electrochemical circuit must be completed within single droplets. We found that amperometric detection was directly applicable to the water-oil two-phase system as long as the length of droplets formed in the microchannel was longer than the microchannel width and than the microelectrodes gap.<sup>6</sup> However, the measurement became complicated when we used ion-selective electrode for droplets. Due to the time needed for ion diffusion and establishing equilibrium on the electrode surface, usually it takes seconds or longer for an ion-selective electrode to provide a stable signal. Under the current experimental conditions, it takes only 0.002 s ~ 0.02 s for one droplet to pass through the two microelectrodes, which is too short to establish stable and measurable signals (Figure 3.5). In addition, the oil in the droplet system interfered with the performance of the ion-selective electrodes, causing large noise in the measurement (Figure 3.5).

### RNA-Mg<sup>2+</sup> Binding Kinetics

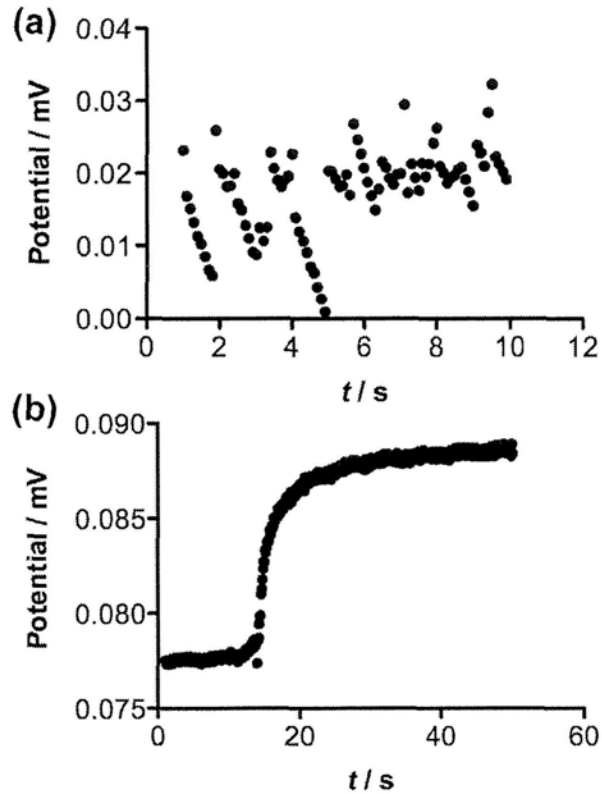


**Figure 3.5** (a) Potential measurement of the droplets in oil by Mg<sup>2+</sup>-selective microelectrode. Potential cannot reach to equilibrium due to the short contacting during when droplets pass through the electrodes. (b) Potential measurement of the droplets by Mg<sup>2+</sup>-selective microelectrode after the oil was separated by the phase separation microchannels.

To solve the above problems, a group of ten parallel 50  $\mu\text{m}$ -wide microchannels were added perpendicularly at the end of the microchannel to separation oil phase and to form a continuous aqueous phase (Figure 3.6).<sup>70, 71</sup> Because the oil phase was separated, the flow rate of droplets was decreasing. The extra time that the droplets spent in the phase separation section was  $\Delta t = L/[v_r(v_r/v_o - 1)]$ , where  $L$  was the length of phase

## RNA-Mg<sup>2+</sup> Binding Kinetics

separation region,  $v_t$  and  $v_o$  were total flow rate and flow rate of oil phase. In our experiment,  $L = 1$  mm,  $v_t = 10 \sim 100$  mm/s and  $v_o = 2 \sim 20$  mm/s, therefore  $\Delta t$  ranged from 0.025 s to 0.0025 s. When the flow rates were constant,  $\Delta t$  was also constant and considered as part of the dead time for the kinetics experiment. By combining phase separation with the droplet-based microfluidic technique, we were able to overcome the intrinsic time limit of the ion-selective electrodes.

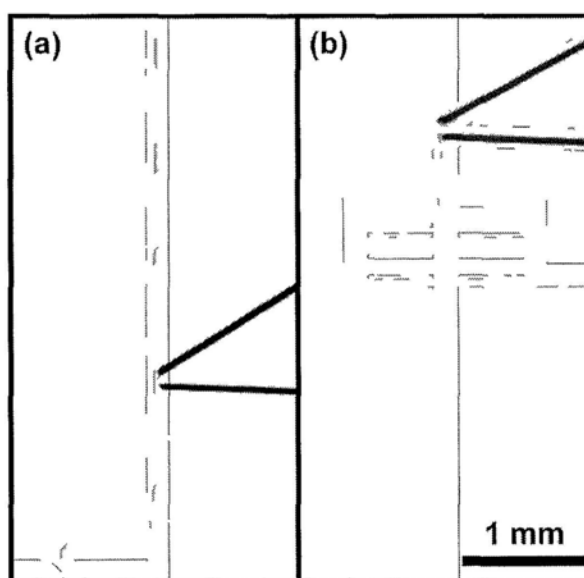


**Figure 3.6** Microphotographs of droplets passing through the two microelectrodes. Microphotographs of droplets passing through the two microelectrodes (a) with and (b) without phase separation channels. The droplets contained  $\text{Fe}(\text{SCN})_x^{(3-x)+}$  for better observation.

### 3.3.2 Analysis of RNA-Mg<sup>2+</sup> binding kinetics

To validate the potentiometric detection-based microfluidic system, we studied the binding kinetics of RNA and Mg<sup>2+</sup>. P4-P6 domain of the *Tetrahymena* group I

## RNA-Mg<sup>2+</sup> Binding Kinetics

ribozyme constructs was tested in the experiment.<sup>69, 72</sup> The P4-P6 domain folds rapidly upon the binding with Mg<sup>2+</sup>.<sup>73</sup> The kinetics was studied by a number of methods, including chemical modification<sup>74</sup>, oligonucleotide hybridization<sup>72, 75</sup>, fluorescence spectrometry<sup>76</sup> and synchrotron hydroxyl radical footprinting.<sup>73</sup> Here by coupling Mg<sup>2+</sup> selective microelectrode in the microfluidic devices, the binding kinetics of the P4-P6 domain and Mg<sup>2+</sup> was studied by monitoring the drop of the Mg<sup>2+</sup> concentration (Figure 3.7). Pneumatic valves were implemented to control the moving distance, i.e. the reaction time of the droplets (Figure 3.4). The Mg<sup>2+</sup> concentration was calculated from a calibration curve using a series of standard Mg<sup>2+</sup> solutions (Figure 3.8). The temporal change of the fraction of Mg<sup>2+</sup> ions that were bound to the P4-P6 domain,  $Y$ , was fit to a two-exponential model  $Y = a(1 - e^{-kt}) + (1 - a)(1 - e^{-k't})$ , where  $k$  and  $k'$  are the first-order rate constants, and  $t$  is reaction time. The two-exponential model significantly improved the fitting quality over the single-exponential model (Figure 3.9), indicating that two Mg<sup>2+</sup> ions were associated with one RNA molecule in a two-step mechanism. Previous crystallographic study and Hill coefficient analysis indicated that five Mg<sup>2+</sup> ions are involved during the folding of each P4-P6 domain.<sup>77, 78</sup> Lately it was suggested that each P4-P6 domain uptakes two Mg<sup>2+</sup> ions upon metal ion core folding while the other Mg<sup>2+</sup> ions diffuse near the RNA molecule without specific binding.<sup>77, 78</sup> The results from the current work agree with the latter model of specific and diffusive binding, as the specific binding reduced the Mg<sup>2+</sup> concentration measured by the ion-selective electrode, while the diffusive binding did not. With the initial reactant concentrations of 0.050 mM Mg<sup>2+</sup> and 0.019 mM RNA, the fast binding rate constant  $k$  was 1.96 s<sup>-1</sup>, and the slow binding rate constant  $k'$  was 0.22 s<sup>-1</sup> (Figure 3.7a, b). When

### RNA-Mg<sup>2+</sup> Binding Kinetics

the initial Mg<sup>2+</sup> and RNA concentrations increased to 0.50 mM and 0.23 mM, respectively,  $k$  increased from 1.96 s<sup>-1</sup> to 3.56 s<sup>-1</sup>, and  $k'$  slightly decreased to 0.15 s<sup>-1</sup> (Figure 3.7c, d). The observed binding kinetics is consistent with previous results of the RNA folding kinetics, which were on the order of 2 s<sup>-1</sup>.<sup>79, 80</sup>

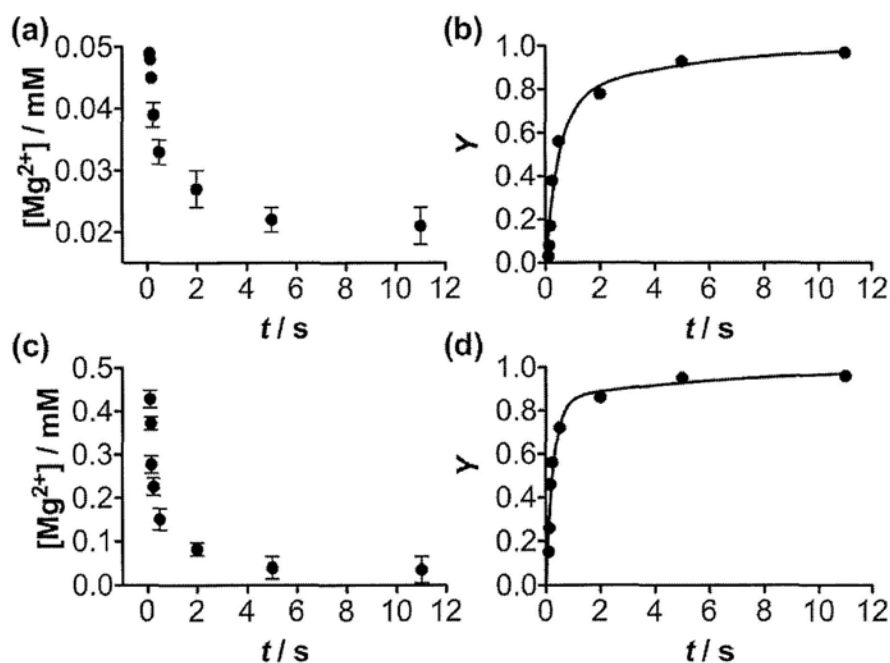


**Figure 3.7** RNA-Mg<sup>2+</sup> binding kinetics results. (a) and (c) The change of free Mg<sup>2+</sup> concentration during the RNA and Mg<sup>2+</sup> binding process. The initial concentrations are (a) 0.050 mM Mg<sup>2+</sup> and 0.019 mM RNA, and (c) 0.50 mM Mg<sup>2+</sup> and 0.23 mM RNA. (b) and (d) The temporal change of the fraction of RNA-Mg<sup>2+</sup> binding reactions  $Y$ .  $Y = ([Mg^{2+}]_i - [Mg^{2+}]_f) / ([Mg^{2+}]_i - [Mg^{2+}]_f)$ , where  $[Mg^{2+}]_f$  and  $[Mg^{2+}]_i$  are the final and initial Mg<sup>2+</sup> concentration in the droplets, respectively. The data points in (b) and (d) are calculated from the data presented in (a) and (c), respectively. The curves are fitting result of a two-exponential model.

### RNA-Mg<sup>2+</sup> Binding Kinetics

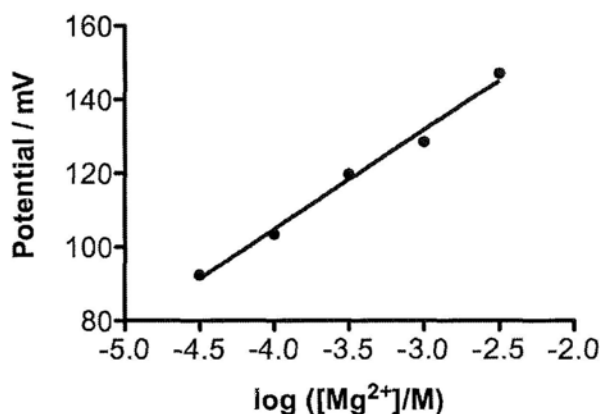


**Figure 3.8** Calibration curve for Mg<sup>2+</sup> concentration measurement ranging from 0.03 mM to 3 mM with the linear fitting of the experimental data. The on-chip calibration was performed on chip using droplets containing know [Mg<sup>2+</sup>] each time before the measurement of the RNA-Mg<sup>2+</sup> binding kinetics. The slope of fitting line is 26.9 mV per ten-fold change of [Mg<sup>2+</sup>], which is a relatively good Nernstian response for the Mg<sup>2+</sup>-selective microelectrode. The best linear range was from 10<sup>-5</sup> mol/L to 10<sup>-1</sup> mol/L, which was adequate to monitor the Mg<sup>2+</sup> ions in the binding kinetics studies.

### RNA-Mg<sup>2+</sup> Binding Kinetics

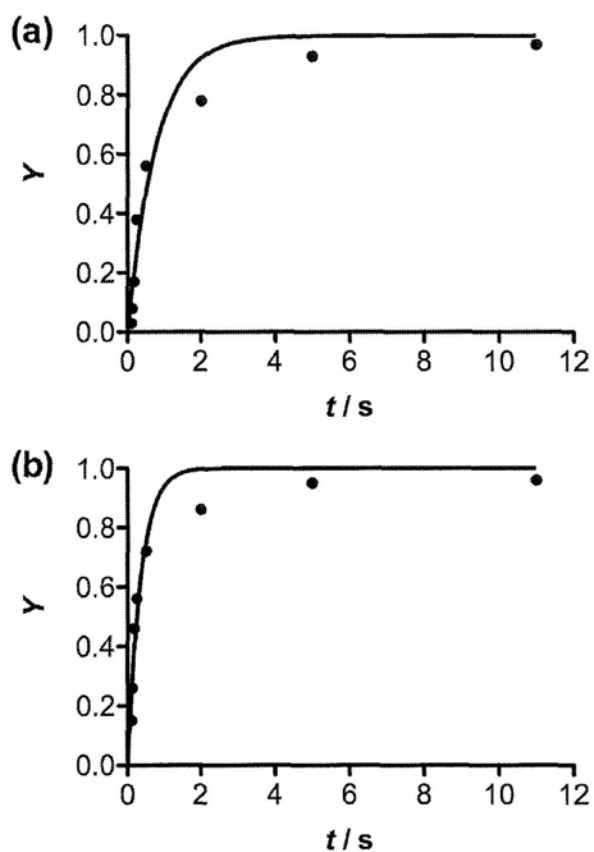


**Figure 3.9** Fitting results of the same data set from **Figure 3.7b, d** with single exponential,  $Y = 1 - e^{-kt}$ . (a) The initial concentrations are 0.050 mM Mg<sup>2+</sup> and 0.019 mM RNA.  $k = 1.3 \text{ s}^{-1}$ ; (b) The initial concentrations are 0.50 mM Mg<sup>2+</sup> and 0.23 mM RNA.  $k = 2.8 \text{ s}^{-1}$ .

## RNA-Mg<sup>2+</sup> Binding Kinetics

### 3.4 Conclusions

In conclusion, we successfully applied potentiometric method to measuring rapid kinetics in droplets in microchannels. Phase separation microchannels were implemented to facilitate potentiometric measurement of the droplets. The system overcomes the intrinsic diffusion time limit of ion-selective electrodes. In this work, RNA-Mg<sup>2+</sup> binding kinetics was studied with the dead time of 0.06 s. The total consumption of RNA was less than 20  $\mu$ L for a single experiment.

The electrodes integrated microfluidic system is complementary to the fluorescence-based microfluidic system for studying biochemical processes. The system has the advantages of inexpensive fabrication and being label-free. We envision the system will find broad applications in studying biochemical reactions that involve small ionic species.

## Conclusions and Perspectives

### Chapter 4 Conclusions and Perspectives

This thesis mainly focused on the application of two major electroanalytical techniques, potentiostatic and potentiometric, in the droplet-based microfluidic systems for rapid kinetics studies. Rapid kinetics measurement is important to understanding many biological and chemical processes, such as protein and RNA folding, protein-protein interaction, and enzymatic mechanism. Droplet-based microfluidic system is a powerful method for kinetics measurement with advantages such as no dispersion, rapid mixing and on-chip dilution. Electrochemistry offers promising techniques particularly attractive for on-chip applications because of the simple equipment, extremely low cost, high compatibility with advanced microfabrication technologies and no need of fluorescence labeling. Enzymatic kinetics and RNA-Mg<sup>2+</sup> binding kinetics were successfully measured by electrochemical detection in the droplet-based microfluidic systems.

In the first part, to avoid the fabrication of an electrode array for monitoring different reaction times, pneumatic valves were implemented to control the reaction time of each droplet. Rapid kinetics of catalase hydrolyzing H<sub>2</sub>O<sub>2</sub> was measured with 0.05 s dead time and less than 50 μL sample consumption. Only one pair of microelectrodes was employed in the microfluidic system, making the PDMS chip simple and inexpensive to fabricate, and the chip can be disposable. This microfluidic system is applicable to many biochemical reactions, as long as one of the reactants or products is electrochemically active.

## Conclusions and Perspectives

Although redox reactions are common and important in biological systems, accurate measurement of the concentration of different ions in biological fluids is also crucial. In the second experiment,  $\text{Mg}^{2+}$ -selective microelectrode was fabricated and implemented in droplet-based microfluidics to measure of the RNA- $\text{Mg}^{2+}$  binding kinetics. A major issue of applying ion-selective electrode in droplet systems is that the equilibrium time of electrodes is too long to have stable signals. To overcome the intrinsic diffusion time limit of ion-selective electrode, phase separation channels were used to separate oil and form single aqueous phase, where the ion-selective electrode can work properly. RNA- $\text{Mg}^{2+}$  binding kinetics was studied with the dead time of 0.06 s. The total consumption of RNA was less than 20  $\mu\text{L}$  for a single experiment. We envision the system will find broad applications in studying biochemical reactions that involve small ionic species.

Electrochemistry is an old branch of chemistry and has mature theory and broad applications in industries. Microfluidic system is a new technology that combines physics, chemistry and engineering to solve problems of bioanalysis. The integration of electrochemistry and microfluidics will have a bright future for the purpose of bioanalytical chemistry, point of care diagnosis and high throughput screening technologies.

## Appendix A

### Appendix A. Fabrication of multilayer microfluidics

#### A.1 Photomask design by AutoCAD

Several graphic design softwares were used to draw the photomask for photolithography, such as Adobe Freehand MX, Adobe Illustrator and AutoCAD. Freehand and Illustrator are similar in terms of function and applications. AutoCAD is a powerful computer aided design software and often used in construction, engineering and architecture designs. AutoCAD is used here for its handy multilayer functions, which help draw and compare two or more layers at the same time. Following are the basic procedures.

1. “PLINE” is always used to form rectangular or arc features to make sure all figures are closed. Because only closed features can be filled when use “HATCH”.
2. For fluid channels, the principles are similar with the design by Freehand.
3. For control channels, try to avoid unnecessary cross-channels. When a channel has to cross a fluid channel below or above, try to use 30  $\mu\text{m}$ -width channels, which will not affect fluid channels. However, it is highly recommended not to use long 30  $\mu\text{m}$  channels, which are relatively difficult to fabricate.
4. Because fluid layer will be fabricated by positive-tone photoresist, channels should be filled with black. In contrast, for negative-tone photoresist, background other than channels should be filled with black.
5. After drawing the design, the structure of multilayer should be decided. One is “push up” structure, where control channels are under the fluid channels (Figure

## Appendix A

A.1). The other is “push down” structure, where control channels are above the fluid channels. “Upper layer” design should be enlarged by **1.015** fold to avoid alignment mismatch caused by thick PDMS elastomer shrinking. “Push up” structure is often used for its higher efficiency of controlling the valves.

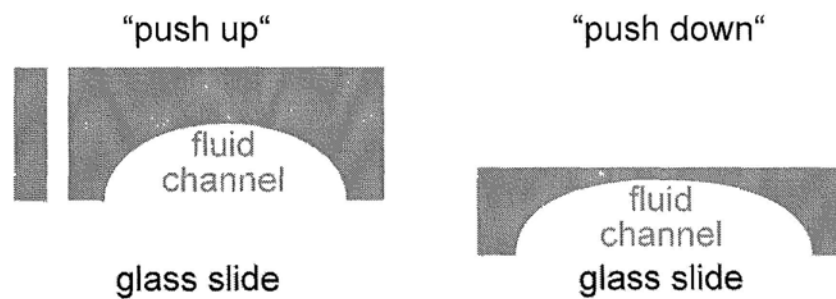


**Figure A.1** “Push up” and “push down” structures.

## Appendix A

### A.2 Photolithography

Photoresists were processed according to manufacturers' suggested protocols for the desired channel pattern thickness (channel depth). AZ P4620 and AZ 50XT positive resists are typically used for fluid-layer molds. Various negative resists of the SU-8 family (MicroChem, Gerstel) are used for control-layer molds.

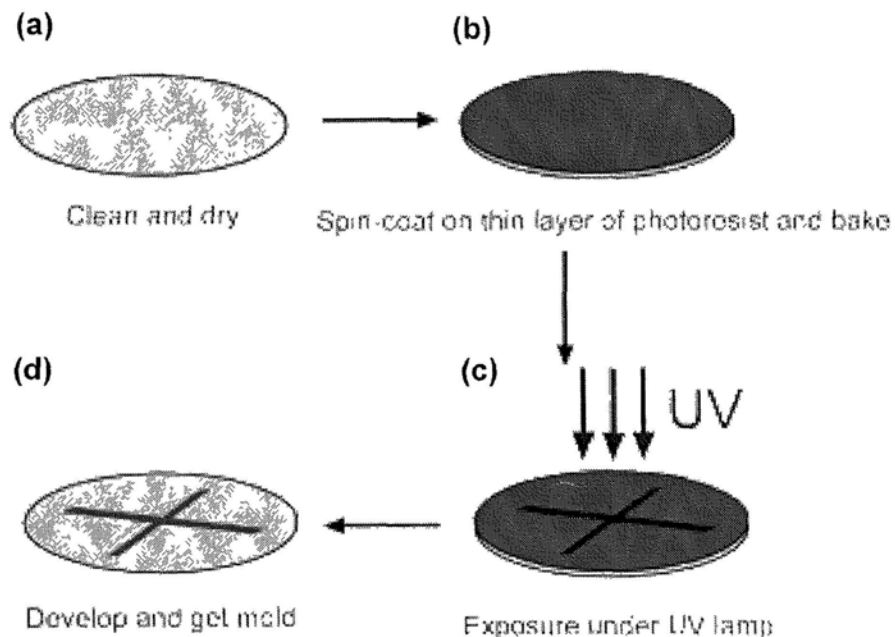


**Figure A.2** Photolithography of AZ photoresist.

The fabrication procedures of round channels by AZ photoresist are as follows.

1. Si wafer pre-treatment (Figure A.2a). Clean the wafers by immersion in piranha solution ( $\text{H}_2\text{SO}_4/\text{H}_2\text{O}_2$  : v/v 3:1) for about 10 min. Then rinse the wafers thoroughly with DI water and dry them by compressed air. Put wafers in 110 °C oven for 30 min to dehydrate the Si wafer. After that, treat surface of Si wafer by using

## Appendix A

- 1,1,1,3,3,3-hexamethyldisilazane (CAS#999-97-3) for about 5 min to enhance the adhesion of AZ photoresist and Si wafer.
2. Spin-coat (Figure A.2b). For AZ P4620 photoresist, 1400 rpm, 60 s, 11~12  $\mu\text{m}$ ; 900 rpm, 60 s, 15  $\mu\text{m}$ . For height > 20  $\mu\text{m}$ , two layers are needed to spin-coat on Si wafer. Remember to spin-coat the second layer after prebake of the first layer.
  3. Prebake: 95°C, 3min then use 115°C for 5 min.
  4. Exposure (Figure A.2c). For the height of 10  $\mu\text{m}$ , the exposure energy is about 400  $\text{mJ}/\text{cm}^2$ .
  5. Caution. There is no post-bake step for AZ photoresist.
  6. Develop (Figure A.2d). Dilute tetramethylammonium hydroxide 1.0 M by DI water (1:3 ~ 1:4 v/v), then put the mold into the solution and develop for about 5 min until clear surface of Si wafer could be observed, then wash with water.
  7. Bake on a hotplate at 150°C for about 1 hour to get the round-shaped mold.

## Appendix A

### A.3 Fabrication of multilayer microfluidic devices

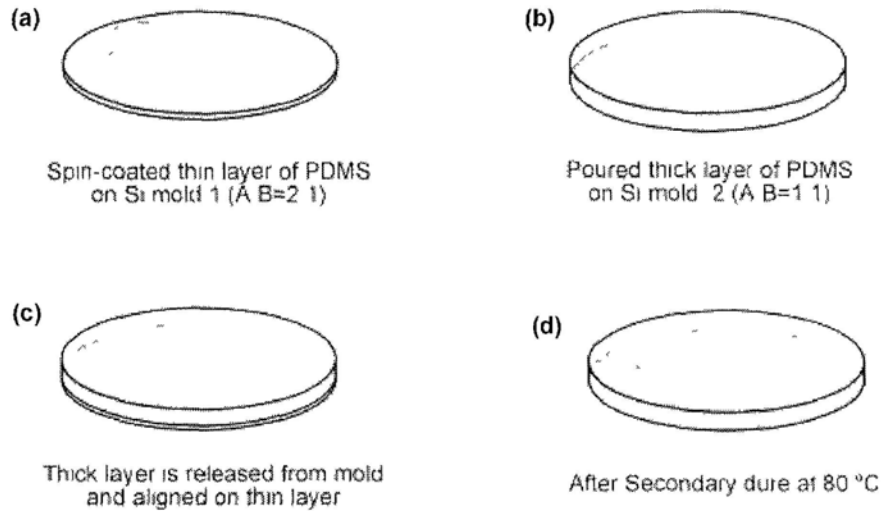


**Figure A.3** Process for making multilayer devices.

1. Silanization. New fabricated masters should be put into petri dishes along with several drops of fluorinated silane under vacuum ( $\sim 72$  mmHg) to do the silanization for about 1~2 hours.
2. Prepare of PDMS. Two different ratio\* of A and B are needed: for the thick layer: A:B=1:1; for the thin layer, A:B=2:1.
3. The thin layer (Figure A.3a). Spin-coat a thin PDMS (A:B=2:1) layer (usually 30  $\mu$ m, 3000 rpm, 150s) onto the Si substrate with control layer SU-8 patterns, then bake in 80 °C oven for 30 min.
4. The thick layer (Figure A.3b). Pour PDMS (A:B=1:1) into Si mold 2 to form a 5~10 mm thick layer. Usually, 20 g PDMS (10 g A and 10 g B) is used for one thick layer. Then whole Petri dish is put into 80 °C oven and bake for 40 min.
5. Substrate. Spin-coat a 50  $\mu$ m PDMS (A:B=2:1) layer onto the glass slide (2000 rpm,

## Appendix A

150s), then baked in 80°C oven for 30min.

6. Bonding. Peel off the thick layer and put it onto the Si wafer with thin layer PDMS, and do the alignment under stereomicroscope carefully and patiently (Figure A.3c). Alignment process can be repeated multiple times until it is correct. Then put them into the 80 °C oven again and bake for an hour to get a monolithic product (Figure A.3d). After the bonding of the first two layers, use tweezers to tear the thin layer PDMS with the thick PDMS slab on top of the Si wafer. Peel off the device that you need and put it onto the glass slide which is coated with thin layer PDMS. Finally, put the whole device into 80 °C oven, stay overnight (>6 hours).

\*A and B are two part PDMS from domestic vendor. Parameters for making devices by Sylgard 184 PDMS are: for thick layer PDMS slab, prepolymer: curing agent = 5:1 and bake for 30 min @ 80 °C; for thin layer PDMS membrane, prepolymer: curing agent = 20:1, spin-coat @ 1500 rpm for 75 s and bake for 30 min @ 80 °C.

## Appendix B

### Appendix B. RNA synthesis

#### B.1 Plasmid DNA cloning

The whole transformation process has to be carried out in 3 days. The following procedures are the cloning of plasmid DNA in DH5 $\alpha$  competent cells.

##### B.1.1 Transformation

###### B.1.1.1 Agar plate preparation

1. Prepare autoclaved LB agar solution. Add 15 mL of the LB agar solution to a 50 mL centrifuge tube. Add 15  $\mu$ L (50 mg/mL) ampicillin to the tube (with fire sterilization).
2. Pour 15 mL LB agar solution with ampicillin to a Petri dish before the agar is solidified at room temperature.

###### B.1.1.2 Transformation

1. Add 1  $\mu$ L of the plasmid DNA to 100  $\mu$ L of DH5 $\alpha$  competent cells in a microtube (without fire sterilization but fast).
2. Place the solution on ice for 20 minutes.
3. Put the solution on a thermomixer to heat it at 42°C for 45 seconds (this time may not be the same according to different competent cells). This is to increase the permeability of the cell membrane so that the vector can enter the cells.

## Appendix B

- Put the solution back on ice for 3 minutes.
- Bend a glass pipette by heating it in fire. Use the pipette to touch the Petri dish cover to cool down the dropper a bit.
- Add the solution (100  $\mu\text{L}$ ) onto the agar plate. Use the bended glass pipette to spread the solution thoroughly on the agar.
- Cover the plate and incubate it at 37°C overnight. Invert the plate upside down to prevent dehydrating the agar.

### B.1.2 Cell culture

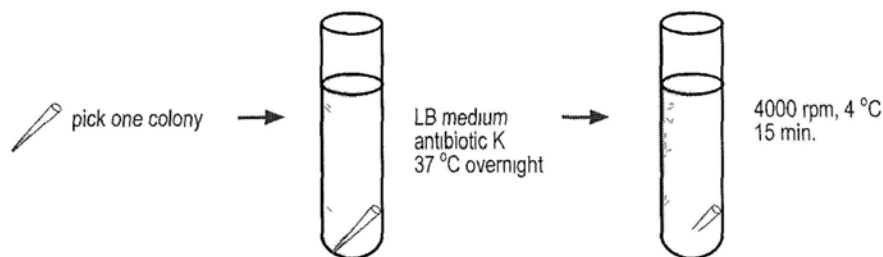


**Figure B.1** Procedures for cell culture.

- Label a 15 mL centrifuge tube and pour 5 mL of 1X LB medium into it. Add 5  $\mu\text{L}$  of ampicillin to the tube with fire sterilization.
- Shake well and use a 10  $\mu\text{L}$  pipette tip to pick one single colony (separate, round, big colony) with fire sterilization.
- Dispose of the pipette tip with bacterial into the centrifuge tube.

## Appendix B

4. Slightly tighten the centrifuge tube. Attach a piece of tape to cover of the tube.  
Incubate the bacterial solution with aeration and agitation at 37°C ~ 8 hours.
5. Spin-down the cells by centrifuging the tube at 4 °C for 4000 ~ 6000 rpm for 15 minutes.
6. After centrifugation, pour away the supernatant and remove as much of the culture medium as you can with micropipette.
7. Store the cells at -20 °C for later use.

### **B.1.3 Plasmid DNA purification by QIAGEN midi preparation kit**

1. Add Buffer P1 to the centrifuge tube containing the harvested pelleted bacteria cells. Pipette up-and-down gently to mix the solution until it becomes homogeneous.
2. Add Buffer P2 to the microtube. Invert the tubes for 4-6 times for mixing the content to lyse the cell.
3. After 5 minutes, add Buffer P3. Invert the tubes for 4-6 times to mix the content.  
This step was to neutralize the lysing action.
4. Centrifuge the tubes at 13000 rpm for 10 minutes with a table-top centrifuge.
5. Preheat 200 µL of Elution Buffer (EB solution) at 50 °C. Preheating the EB solution may increase the yield.

## Appendix B

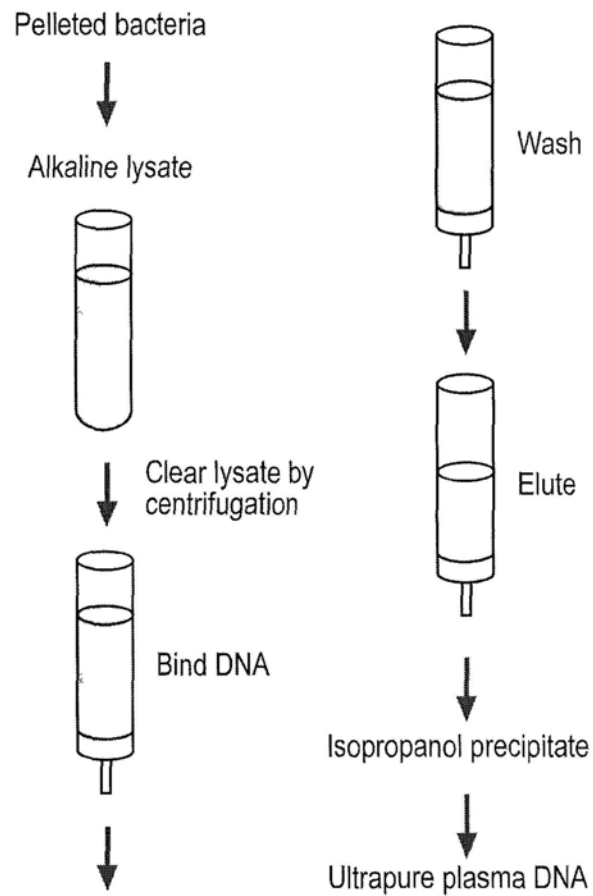


**Figure B.2** Procedures of plasmid DNA purification.

6. After centrifugation, white precipitate would be formed and would be stuck on the wall or at the bottom of the microtubes. Transfer only the supernatant to the 3 spin-columns and avoid transferring the precipitate.
7. Without covering the column, centrifuge it at maximum speed for 60 seconds.
8. Remove the supernatant. Add 750  $\mu\text{L}$  of Buffer PE (with ethanol added) to the spin-column.
9. Centrifuge the column without covering at maximum speed for 60 seconds.

## **Appendix B**

10. Discard the supernatant. Centrifuge the empty spin-column for 60 seconds. This step was to remove the residual buffer.

11. Transfer the columns to a new 1.5 mL microtube. Add 50  $\mu$ L of preheated EB solution\*. Let it stand for 60 seconds at room temperature. Centrifuge it at maximum speed for 60 seconds. The resulting solution was the product.

\* The volume used can be adjusted according to the final concentration. Preheated DI water can be used to replace EB solution.

## Appendix B

### B.2 RNA transcription and purification

#### B.2.1 Transcription by MEGAscript kit

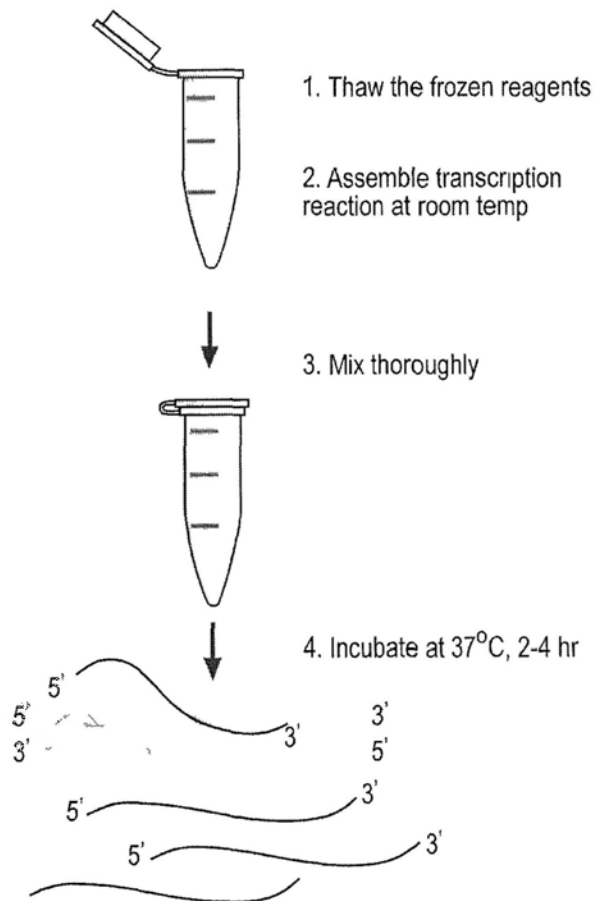


**Figure B.3** Procedures of RNA transcription by MEGAscript kit.

1. Thaw the frozen reagents
  - a. Place the RNA Polymerase Enzyme Mix on ice, it is stored in glycerol and will not be frozen at  $-20^{\circ}\text{C}$ .

## Appendix B

- b. Vortex the 10X Reaction Buffer and the 4-ribonucleotide solutions (ATP, CTP, GTP, and UTP) until they are completely in solution. Once thawed, store the ribonucleotides on ice, but keep the 10X Reaction Buffer at room temperature while assembling the reaction.
  - c. All reagents should be microfuged briefly before opening to prevent loss and contamination of material that may be present around the rim of the tube.
2. Assemble transcription reaction at room temp
    - a. The spermidine in the 10X Reaction Buffer can co-precipitate the template DNA if the reaction is assembled on ice.
    - b. Add the 10X Reaction Buffer after the water and the ribonucleotides are already in the tube.
    - c. The following amounts are for a single 20  $\mu$ L reaction. Reactions may be scaled up or down if desired.
  3. Mix thoroughly

Gently flick the tube or pipette the mixture up and down gently, and then microfuge tube briefly to collect the reaction mixture at the bottom of the tube.
  4. Incubate at 37 °C, 2 ~ 4 hrs.
    - a. The first time a new template is transcribed, the recommended incubation time is 2~4 hours. The optimal incubation time for a given template will

## Appendix B

vary depending on the size and transcriptional efficiency of your template. For short transcripts (less than 500 nt), a longer incubation time (up to ~16 hours) may be advantageous, since more transcription initiation events are required to synthesize a given mass amount of RNA, compared to transcription of longer templates.

- b. To determine the optimum incubation time for maximum yield with a given template, a time-course experiment can be done. To do this, set up a MEGAscript reaction, and remove aliquots of the reaction at various intervals (for example after 1, 2, 4, or 6 hours, and overnight incubation). Assess results by TCA precipitation or other means.
5. Add 1  $\mu$ L TURBO DNase, mix well and incubate 15 min at 37°C. (optional)
    - a. This DNase treatment removes the template DNA. For many applications it may not be necessary because the template DNA will be present at a very low concentration relative to the RNA.
    - b. Add 1  $\mu$ L TURBO DNase, and mix well (the reaction may be viscous).
    - c. Incubate at 37°C for 15 min.

### **B.2.2 RNA Purification by MEGAclear kit**

Centrifuge method was used in the experiment to purify the RNA samples.

1. Mix the RNA sample with 100  $\mu$ L with Elution Solution.

## Appendix B

2. Add 350  $\mu\text{L}$  of Binding Solution Concentrate to the sample and mix gently by pipetting.
3. Add 250  $\mu\text{L}$  of 100% ethanol to the sample and mix gently by pipetting.
4. Apply the sample to the filter.
  - a. Insert a Filter Cartridge into one of the Collection and Elution Tubes supplied.
  - b. Pipet the RNA mixture onto the Filter Cartridge.
  - c. Centrifuge for  $\sim 15$  sec to 1 min, or until the mixture has passed through the filter. Centrifuge at RCF 10,000  $\sim$  15,000  $\times$  g (typically 10,000  $\sim$  14,000 rpm). Spinning harder than this may damage the filters.
  - d. Discard the flow-through and reuse the Collection and Elution Tube for the washing steps.
5. Wash with 2  $\times$  500  $\mu\text{L}$  Wash Solution.

Make sure that the ethanol has been added to the Wash Solution Concentrate before using it.

- a. Apply 500  $\mu\text{L}$  Wash Solution. Draw the Wash Solution through the filter as in the previous step.
- b. Repeat with a second 500  $\mu\text{L}$  aliquot of Wash Solution.

## Appendix B

- c. After discarding the Wash Solution, continue centrifugation or leave the Filter Cartridge on the vacuum manifold for 10~30 sec to remove the last traces of Wash Solution.

### 6. Elute RNA with 50 $\mu$ L Elution Solution.

Elute the RNA from the filter using either one of the methods described below; they are equivalent in terms of RNA recovery.

- a. Place the Filter Cartridge into a new Collection/Elution Tube.
- b. Apply 50  $\mu$ L of Elution Solution to the center of the Filter Cartridge. Close the cap of the tube and incubate in a heat block set to 65~70°C for 5–10 min.
- c. Recover eluted RNA by centrifuging for 1 min at RT (RCF 10,000~15,000  $\times$  g).
- d. To maximize RNA recovery, repeat this elution procedure with a second 50  $\mu$ L aliquot of Elution Solution. Collect the elute into the same tube.

## Appendix B

### B.3 RNA experiment preparation

#### B.3.1 RNase-free water

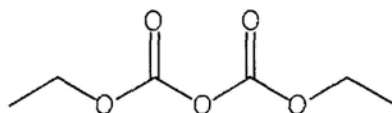


**Figure B.4** Structure of diethylpyrocarbonate, DEPC.

Water is treated with 0.1% v/v diethylpyrocarbonate for 1 hour at 37°C and then autoclaved (~ 15 min) to inactivate traces of DEPC. Inactivation of DEPC in this manner yields CO<sub>2</sub>, H<sub>2</sub>O and ethanol. Higher concentrations of DEPC are competent of deactivating larger amounts of RNase but remaining traces or byproducts may inhibit further biochemical reactions such as *in vitro* translation. Further on, chemical modification of RNA such as carboxymethylation is possible when traces of DEPC or its byproducts are present, resulting to reduced usage of RNA even after buffer exchange (after precipitation).

#### B.3.2 other precautions

1. Clean the lab bench and micropipettes with DEPC solution as often as possible.
2. Wear laboratory gloves at all and change them frequently. They will protect you from the reagents, and they will protect the RNA from nucleases that are present on skin.
3. Always use RNase-free pipette tips and microfuge tubes.

## References

## References

1. Quack, M., *Chimia* **2003**, *57*, 147-160.
2. Khorasanizadeh, S.; Peters, I. D.; Butt, T. R.; Roder, H., *Biochemistry* **1993**, *32*, 7054-7063.
3. Olson, S. T.; Bjork, I., *J. Biol. Chem.* **1991**, *266*, 6353-6364.
4. Eyles, S. J.; Radford, S. E.; Robinson, C. V.; Dobson, C. M., *Biochemistry* **1994**, *33*, 13038-13048.
5. Kane, D. J.; Fendler, K.; Grell, E.; Bamberg, E.; Taniguchi, K.; Froehlich, J. P.; Clarke, R. J., *Biochemistry* **1997**, *36*, 13406-13420.
6. Han, Z. Y.; Li, W. T.; Huang, Y. Y.; Zheng, B., *Anal. Chem.* **2009**, *81*, 5840-5845.
7. Knight, J. B.; Vishwanath, A.; Brody, J. P.; Austin, R. H., *Phys. Rev. Lett.* **1998**, *80*, 3863-3866.
8. Pollack, L.; Tate, M. W.; Darnton, N. C.; Knight, J. B.; Gruner, S. M.; Eaton, W. A.; Austin, R. H., *Proc. Natl. Acad. Sci. U. S. A.* **1999**, *96*, 10115-10117.
9. Song, H.; Ismagilov, R. F., *J. Am. Chem. Soc.* **2003**, *125*, 14613-14619.
10. Duffy, D. C.; McDonald, J. C.; Schueller, O. J. A.; Whitesides, G. M., *Anal. Chem.* **1998**, *70*, 4974-4984.
11. Xia, Y. N.; Whitesides, G. M., *Angew. Chem.-Int. Edit.* **1998**, *37*, 551-575.
12. Qin, D.; Xia, Y. N.; Whitesides, G. M., *Nat Protoc* **2010**, *5*, 491-502.
13. Kumar, A.; Whitesides, G. M., *Appl. Phys. Lett.* **1993**, *63*, 2002-2004.

## References

14. Xia, Y. N.; Kim, E.; Zhao, X. M.; Rogers, J. A.; Prentiss, M.; Whitesides, G. M., *Science* **1996**, *273*, 347-349.
15. Zhao, X. M.; Xia, Y. N.; Whitesides, G. M., *Adv. Mater.* **1996**, *8*, 837-840.
16. Kim, E.; Xia, Y. N.; Whitesides, G. M., *Nature* **1995**, *376*, 581-584.
17. Kim, E.; Xia, Y. N.; Zhao, X. M.; Whitesides, G. M., *Adv. Mater.* **1997**, *9*, 651-654.
18. Unger, M. A.; Chou, H. P.; Thorsen, T.; Scherer, A.; Quake, S. R., *Science* **2000**, *288*, 113-116.
19. Thorsen, T.; Maerkl, S. J.; Quake, S. R., *Science* **2002**, *298*, 580-584.
20. Hansen, C. L.; Skordalakes, E.; Berger, J. M.; Quake, S. R., *Proc. Natl. Acad. Sci. U. S. A.* **2002**, *99*, 16531-16536.
21. Bird, R. B.; Stewart, W. E.; Lightfoot, E. N., *Transport phenomena*. 2nd, Wiley international ed.; J. Wiley: New York, 2002.
22. Song, H.; Tice, J. D.; Ismagilov, R. F., *Angew. Chem.-Int. Edit.* **2003**, *42*, 768-772.
23. Aharoni, A.; Griffiths, A. D.; Tawfik, D. S., *Curr Opin Chem Biol* **2005**, *9*, 210-216.
24. Bernath, K.; Hai, M. T.; Mastrobattista, E.; Griffiths, A. D.; Magdassi, S.; Tawfik, D. S., *Anal Biochem* **2004**, *325*, 151-157.
25. Dobson, C. M., *Nature* **2004**, *432*, 824-828.
26. Stroock, A. D.; Dertinger, S. K. W.; Ajdari, A.; Mezic, I.; Stone, H. A.; Whitesides, G. M., *Science* **2002**, *295*, 647-651.

## References

27. Pollack, L.; Tate, M. W.; Finnefrock, A. C.; Kalidas, C.; Trotter, S.; Darnton, N. C.; Lurio, L.; Austin, R. H.; Batt, C. A.; Gruner, S. M.; Mochrie, S. G. J., *Phys. Rev. Lett.* **2001**, *86*, 4962-4965.
28. Song, H.; Bringer, M. R.; Tice, J. D.; Gerdts, C. J.; Ismagilov, R. F., *Appl. Phys. Lett.* **2003**, *83*, 4664-4666.
29. Wang, J.; Tian, B.; Sahlin, E., *Anal. Chem.* **1999**, *71*, 5436-5440.
30. Hilmi, A.; Luong, J. H. T., *Anal. Chem.* **2000**, *72*, 4677-4682.
31. Martin, R. S.; Gawron, A. J.; Lunte, S. M.; Henry, C. S., *Anal. Chem.* **2000**, *72*, 3196-3202.
32. Woolley, A. T.; Lao, K.; Glazer, A. N.; Mathies, R. A., *Anal. Chem.* **1998**, *70*, 684-688.
33. Gavin, P. F.; Ewing, A. G., *Anal. Chem.* **1997**, *69*, 3838-3845.
34. Erickson, D.; Li, D. Q., *Anal. Chim. Acta* **2004**, *507*, 11-26.
35. Kurita, R.; Hayashi, K.; Fan, X.; Yamamoto, K.; Kato, T.; Niwa, O., *Sens. Actuator B-Chem.* **2002**, *87*, 296-303.
36. Moser, I.; Jobst, G.; Urban, G. A., *Biosens. Bioelectron.* **2002**, *17*, 297-302.
37. Cai, X. X.; Klauke, N.; Glidle, A.; Cobbold, P.; Smith, G. L.; Cooper, J. M., *Anal. Chem.* **2002**, *74*, 908-914.
38. Wu, J.; Suls, J.; Sansen, W., *Sens. Actuator B-Chem.* **2001**, *78*, 221-227.
39. Lindsay, S.; Vazquez, T.; Egatz-Gomez, A.; Loyprasert, S.; Garcia, A. A.; Wang, J., *Analyst* **2007**, *132*, 412-416.
40. Zhan, Y. H.; Wang, J.; Bao, N.; Lu, C., *Anal. Chem.* **2009**, *81*, 2027-2031.

## References

41. Luo, C. X.; Yang, X. J.; Fu, O.; Sun, M. H.; Ouyang, Q.; Chen, Y.; Ji, H., *Electrophoresis* **2006**, *27*, 1977-1983.
42. Liu, S. J.; Gu, Y. F.; Le Roux, R. B.; Matthews, S. M.; Bratton, D.; Yunus, K.; Fisher, A. C.; Huck, W. T. S., *Lab Chip* **2008**, *8*, 1937-1942.
43. Lehninger, A. L.; Nelson, D. L.; Cox, M. M., *Lehninger principles of biochemistry*. 5th ed.; W.H. Freeman: New York, 2008.
44. Bringer, M. R.; Gerdt, C. J.; Song, H.; Tice, J. D.; Ismagilov, R. F., *Philos. Trans. R. Soc. Lond. Ser. A-Math. Phys. Eng. Sci.* **2004**, *362*, 1087-1104.
45. Lingane, J. J.; Lingane, P. J., *J. Electroanal. Chem.* **1963**, *5*, 411-419.
46. Garstecki, P.; Fuerstman, M. J.; Stone, H. A.; Whitesides, G. M., *Lab Chip* **2006**, *6*, 437-446.
47. Tice, J. D.; Song, H.; Lyon, A. D.; Ismagilov, R. F., *Langmuir* **2003**, *19*, 9127-9133.
48. Evans, S. A. G.; Elliott, J. M.; Andrews, L. M.; Bartlett, P. N.; Doyle, P. J.; Denuault, G., *Anal. Chem.* **2002**, *74*, 1322-1326.
49. Hall, S. B.; Khudaish, E. A.; Hart, A. L., *Electrochim. Acta* **1997**, *43*, 579-588.
50. Nakanishi, S.; Mukoyama, Y.; Karasumi, K.; Imanishi, A.; Furuya, N.; Nakato, Y., *J. Phys. Chem. B* **2000**, *104*, 4181-4188.
51. Zhang, Y.; Wilson, G. S., *J. Electroanal. Chem.* **1993**, *345*, 253-271.
52. Nicholls, P.; Fita, I.; Loewen, P. C., *Enzymology and structure of catalases*. Academic Press Inc: San Diego, 2001.
53. Switala, J.; Loewen, P. C., *Arch. Biochem. Biophys.* **2002**, *401*, 145-154.

## References

54. Lin, Y.; Gerfen, G. J.; Rousseau, D. L.; Yeh, S. R., *Anal. Chem.* **2003**, *75*, 5381-5386.
55. Kremp, D.; Beskrownij, W., *J. Chem. Phys.* **1996**, *104*, 2010-2017.
56. Hill, T. L., **1955**, *23*, 623-636.
57. Laing, L. G.; Gluick, T. C.; Draper, D. E., *J. Mol. Biol.* **1994**, *237*, 577-587.
58. Anderson, C. F.; Record, M. T., *Annu. Rev. Phys. Chem.* **1995**, *46*, 657-700.
59. Conway, B. E., *Ionic hydration in chemistry and biophysics*. Elsevier Scientific Pub. Co. : distributors for the U.S. and Canada, Elsevier/North-Holland: Amsterdam ; New York, 1981.
60. Bockris, J. O. M.; Reddy, A. K. N.; Gamboa-Aldeco, M. E., *Modern electrochemistry*. 2nd ed.; Plenum Press: New York, 1998.
61. Jayaram, B.; Sharp, K. A.; Honig, B., *Biopolymers* **1989**, *28*, 975-993.
62. Misra, V. K.; Honig, B., *Biochemistry* **1996**, *35*, 1115-1124.
63. Sharp, K. A.; Honig, B.; Harvey, S. C., *Biochemistry* **1990**, *29*, 340-346.
64. Shui, X. Q.; McFail-Isom, L.; Hu, G. G.; Williams, L. D., *Biochemistry* **1998**, *37*, 8341-8355.
65. Zana, R.; Tondre, C., **1974**, *1*, 367-375.
66. Celander, D. W.; Cech, T. R., *Science* **1991**, *251*, 401-407.
67. Grosshans, C. A.; Cech, T. R., *Biochemistry* **1989**, *28*, 6888-6894.
68. Laggerbauer, B.; Murphy, F. L.; Cech, T. R., *Embo J.* **1994**, *13*, 2669-2676.
69. Das, R.; Travers, K. J.; Bai, Y.; Herschlag, D., *J. Am. Chem. Soc.* **2005**, *127*, 8272-8273.
70. Castell, O. K.; Allender, C. J.; Barrow, D. A., *Lab Chip* **2009**, *9*, 388-396.

## References

71. Kralj, J. G.; Sahoo, H. R.; Jensen, K. F., *Lab Chip* **2007**, *7*, 256.
72. Treiber, D. K.; Rook, M. S.; Zarrinkar, P. P.; Williamson, J. R., *Science* **1998**, *279*, 1943-1946.
73. Sclavi, B.; Sullivan, M.; Chance, M. R.; Brenowitz, M.; Woodson, S. A., *Science* **1998**, *279*, 1940-1943.
74. Banerjee, A. R.; Turner, D. H., *Biochemistry* **1995**, *34*, 6504-6512.
75. Zarrinkar, P. P.; Williamson, J. R., *Science* **1994**, *265*, 918-924.
76. Silverman, S. K.; Cech, T. R., *Biochemistry* **1999**, *38*, 14224-14237.
77. Cate, J. H.; Hanna, R. L.; Doudna, J. A., *Nat. Struct. Biol.* **1997**, *4*, 553-558.
78. Chen, S. J., *Ann. Rev. Biophys.* **2008**, *37*, 197-214.
79. Silverman, S. K.; Deras, M. L.; Woodson, S. A.; Scaringe, S. A.; Cech, T. R., *Biochemistry* **2000**, *39*, 12465-12475.
80. Deras, M. L.; Brenowitz, M.; Ralston, C. Y.; Chance, M. R.; Woodson, S. A., *Biochemistry* **2000**, *39*, 10975-10985.